ROYAL IHC

Vibration isolation for deck-mounted superstructures

Applied to Cutter Suction Dredgers

L. van der Meer

4/20/2016

Graduation committee:	Prof. dr. A. Metrikine	TU Delft - Chairman
	Dr. ir. A. Tsouvalas	TU Delft
	Ir. J.G. Los	Royal IHC
	Dr. ir. K van Dalen	TU Delft
University:	Delft University of Technology	
Faculty:	Mechanical, Maritime and Materials Engineering	
Program:	Offshore and Dredging Engineering	
Master track:	Bottom Founded Structures	
Date:	April 2016	

Author: *Lieuwe van der Meer*

Contact: *Lieuwevdmeer@gmail.com*

This thesis is confidential and cannot be made public until April 20, 2018

Preface

This report contains the results of a study into vibration isolation for deck mounted superstructures specifically applied to cutter suction dredgers. The research is part of a master thesis for the study Offshore and Dredging Engineering at the Delft University of Technology.

The research is performed for Royal IHC and in collaboration with the Delft university of Technology. I would like to thank these institutes and especially my graduation committee: Prof. dr. A. Metrikine, dr. ir. A. Tsouvalas, ir. J.G. Los and dr. ir. K van Dalen for their ideas, comments, time and enthousiasm. Especially ir. J.G. Los and dr. ir. A. Tsouvalas have earned my gratitude for their day to day support and detailed reviewing.

I would also like to thank Royal IHC as a whole, IHC MTI and IHC Ddredgers specifically for giving me the opportunity to do my thesis at the departments that were affected by the thesis. Many thanks for the warm welcome I've received and for the information that was made available for my thesis.

Delft, April 2016

Lieuwe van der Meer

Abstract

The majority of Cutter Suction Dredge (CSD) vessels (Figure 1) is equipped with rubber isolators for Operator Cabin (OC) vibration reduction. A small number of vessels is equipped with expensive gas springs. Of the vessels that have been equipped with rubber isolators, a number is experiencing large vibrations caused by what is assumed resonance between the OC and the vessel. This research focuses on the development of an economically feasible solution to reduce vibrations for deck-mounted superstructures in CSDs.

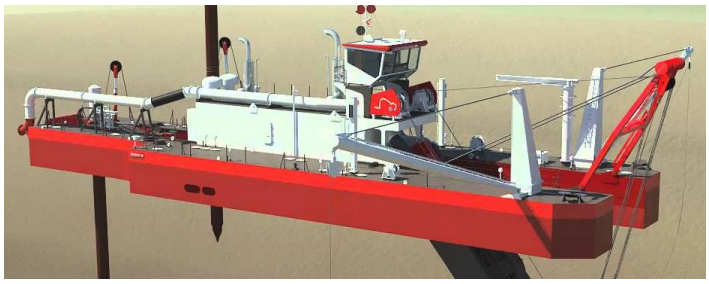

Figure 1, Cutter suction dredger

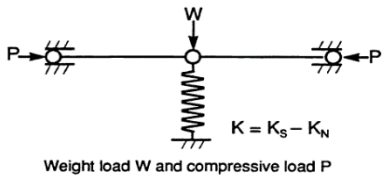

Figure 2, Negative stiffness mechanism

In the first part of the thesis the focus was placed on investigating the driving frequencies in CSDs and the natural frequencies of the coupled OC-vessel system. For this purpose, a model was developed and it was found that the large amplitude motions were in fact caused by resonance of the system in one of the driving frequencies. To solve this problem several solutions were studied. The initial investigation resulted in the proposal of a low-frequency vibration isolation using a load bearing spring combined with a Negative Stiffness Mechanism (NSM)(Figure 2).

The NSM was modelled to verify the behaviour of the NSM and the OC – vessel system and the design parameters were obtained. To validate the proposed concept, a prototype was constructed (Figure 3). The prototype shows that during the detailed design stage the influence of friction and the influence of tolerances have to be minimised.

Figure 3, Prototype

The next steps in the development of the NSM as a product will need to centre around a 6DOF prototype set up and the detailed design of the internal mechanism of the NSM. This includes material selection, profile selection and design of the hinge points.

Table of Contents

Table of Figures

1 Problem Statement

IHC encountered a number of problems with vibration isolation on beaver type cutter suction dredgers. The main problems occurred in the plate fields, the discharge pipelines and the operating cabins. Since not all of the aforementioned issues can be addressed in this thesis due to time limitations, the focus will be placed on the vibration isolation of the operating cabins alone.

1.1 Cutter Suction Dredgers

A cutter suction dredger (CSD) consists of a pontoon, a cutter, the spuds, the machinery, the piping and the housing. A CSD is in essence a large floating drill; vibrations are inherent in the functioning of such a vessel. An example of a small beaver type CSD is shown in Figure 1-1.

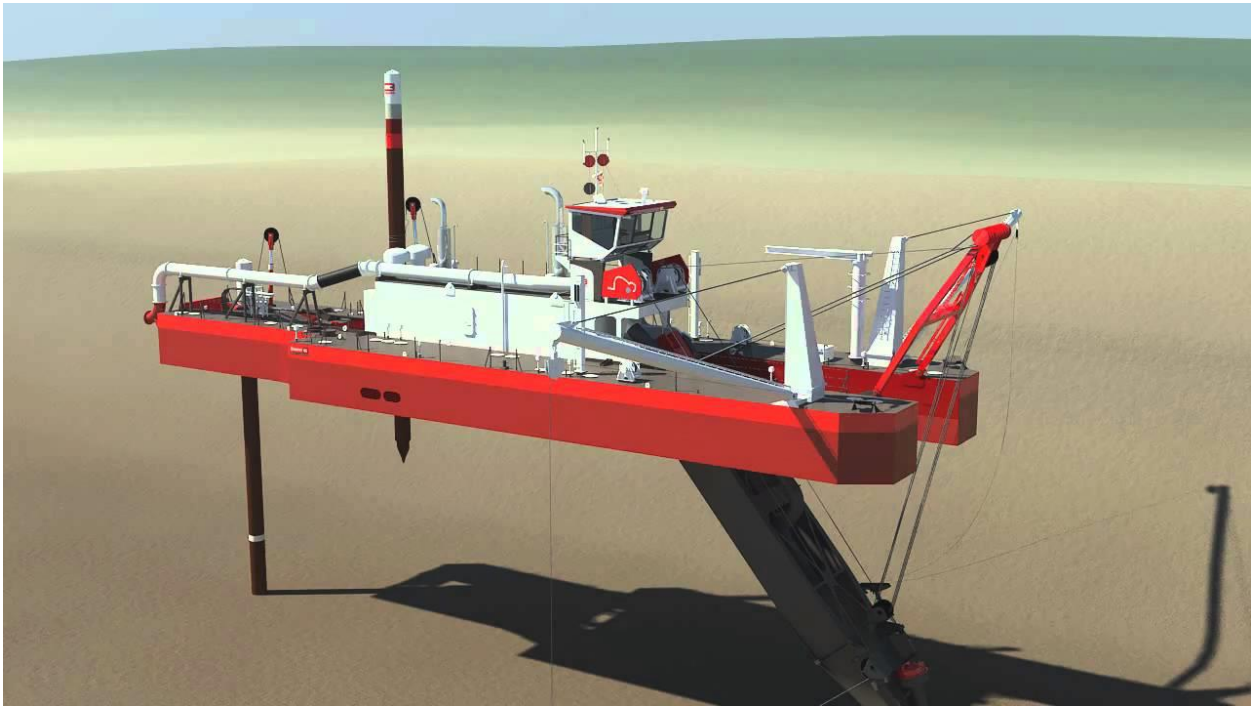

Figure 1-1, Beaver 50 CSD (Royal IHC, MTI)

These vessels are available in different sizes and at different costs. What all the vessels have in common is the Operator Cabin (OC) in which the dredge master is operating the vessel. Some have an Accommodation block (AC) where the crew can rest and have meals. Vibrations in these areas can be detrimental to health, safety, productivity and wear. Thus, it is important to keep the vibration amplitudes to within allowable levels.

1.2 Background

The dredging industry is becoming a more mature market. On the one hand, dredging vessels are no longer a one of a kind project, but are standardised to allow cheaper production. On the other hand, clients have increased demands. This means in practice that the standardised cutter vessels are outfitted with more power and heavier cutters to meet these demands. The increased power allows the cutters to dredge harder material types such as rock but leads to increased vibrations in the vessel deck, and

consequently in the deck-mounted super structures, such as the operating cabin and the accommodation block. Increasing comfort demands for the crew and minimisation of the induced vibrations by the cutter lead to an increased focus on vibration isolation.

1.3 IHC solutions

In the past CSD vessels were built without any form of passive or active vibration isolation systems and all parts were welded together into a single piece. However, in the recent years this trend is slowly abandoned. Recently, IHC has been working on the reduction of the induced vibrations. All the new CSD vessels are delivered with some type of vibration amplitude reduction. The standard design for these measures is the implementation of rubber profiles between the OC and the supports, an example of such a system is shown in Figure 1-2.

Figure 1-2, OC on rubber (Royal IHC, MTI)

Most of the Beaver Dredgers designed, built and delivered by IHC with the rubber suspension have received no complaints about excessive vibrations. This does not necessarily mean that there were no vibration issues, but since no data regarding the vibration amplitudes is collected, these vessels cannot be analysed in this thesis. Several vessels, however, have shown some undesired vibrations despite the fact that some form of vibration isolation (reduction) has been *a priori* applied. One of the better documented cases is the Shanti Sagar XVI. The Shanti Sagar is a vessel constructed by IHC and delivered in 2013 to the client.

In the case of the Shanti Sagar, the vibrations in the operating cabin were quite severe. The vibrations in the OC were even larger than the vibrations in the deck. This increase in vibration amplitude indicates that the originally designed vibration reduction system turned out to be a vibration amplification system.

To minimise the vibration amplitudes the crew on board tried to apply some ratchet straps from the deck to the top of the cabin. This reduced the amplitude of vibrations somewhat but not to a satisfactory level. Since IHC constructed the vessel and suspension, IHC was contacted to fix the problem.

Figure 1-3, Shanti Sagar, ratchet straps (Royal IHC, MTI)

Figure 1-4, Shanti Sagar close up of ratchet strap (Royal IHC, MTI)

The solution of the IHC representative was then to solve the problem by replacing the rubber suspension system with steel struts. Effectively removing the suspension system and restricting the vibrations to the deck vibrations. By doing this the higher frequency machine vibrations that actually were reduced by the rubber suspension were amplified. In other words, the low frequency motions were effectively reduced by the steel struts but the higher frequency components were amplified instead. Thus, the problem was solved only partly.

In another case, the large custom built CSDs Arthemis and Athena for van Oord, the issues were known and were considered by a design team. To prevent the excessive vibration issues a very expensive air spring system was used. This system, while expensive, functions excellently. However, for the smaller serial produced vessels these high costs are prohibitive.

Figure 1-5, Air spring suspenders

1.4 Research goals

The main goals of the thesis are:

- To determine why the rubber isolators currently installed on the vessel are amplifying the vibrations.
- To reduce the vibrations currently experienced by the crew
- To help IHC prevent issues in the future by providing a design guide for the engineering department and provide and alternative for the current isolation systems

The thesis focuses on providing a cost effective and functioning replacement for the current suspension system and a guideline for the IHC design team on the design of these vibration reduction systems.

1.5 Method

The OC is assumed to be a rigid body with six Degrees of Freedom (6 DoF) coupled with linear springs to the vessel. Since the ratio of the mass of the OC to the mass of the vessel is small, one can assume that there is no vessel-OC interaction. The assumptions allow for the use of linear dynamic theory on a single rigid body with a base excitation for the OC – vessel system.

First, an investigation was done into the possible driving frequencies inherent in cutter suction dredgers. The second investigation was into the natural frequencies of the OC – vessel system. The combination of driving and natural frequencies led to the solution of choice to be low frequency vibration isolation to reduce the vibrations in the OC effectively.

The options for low frequency vibration isolation for CSDs are limited to gas springs and a stiff load bearing spring combined with a Negative Stiffness Mechanism (NSM). Gas springs are deemed too expensive by the client, therefore an NSM is preferred.

A large number of possible designs can be made for an NSM. The design used in this study is a spring loaded rigid bar type. The NSM of choice is modelled in 1 DoF to verify the behaviour of the NSM. A 6 DoF model is used to verify the behaviour of the OC – vessel system. The design and scaling parameters are obtained from the 1 DoF model.

To validate the previous discussed method and assumptions a 1 DoF physical prototype was constructed. The prototype was used to determine whether the low damping, geometrical relations and the operation of the NSM would be the same as the theory.

1.6 Thesis layout

Chapter 1: Problem statement

Chapter 2: Literature study

Chapter 3: Inventory

Chapter 4: Modelling

Chapter 5: Practical implementation

Chapter 6: Conclusions

2 Literature Study

This chapter discusses the basic dynamics topics and the various methods of vibration amplitude reduction and how they can be applied to the problem. The dynamics are derived from several pieces of literature, courses and lecture slides. (Meriam, 1998) (Spijkers, 2005)

2.1 Dynamics of a SDOF system

The basis of the dynamics is the single degree of freedom system as shown in Figure 2-1. This is the simplest way to represent the OC subjected to some base excitation from the vessel. No vessel-OC interaction is assumed because the difference in mass is significant. The system consists of a mass $[m]$, a spring coefficient $[k]$ and a damping coefficient $[c]$. The mass and the base can move. The motions of the base can be prescribed by a function $x_b(t)$. The motion of the mass can be found by solving the differential equation for $x(t)$.

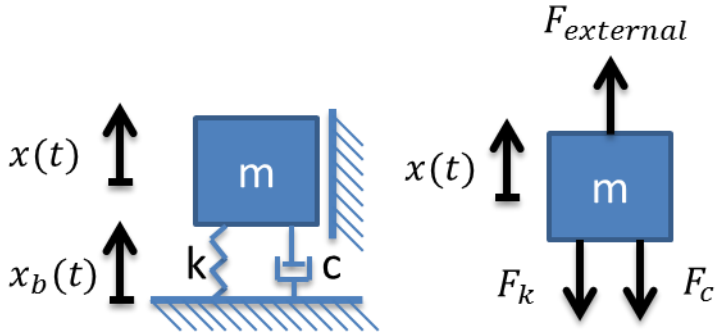

Figure 2-1, Single degree of freedom system and free body diagram

The movement of the mass is restricted in all directions other than the vertical direction. Solving the equation of motion can be separated in the natural motions of the system. The motions are called the transient motions.

2.1.1 Free vibrations

In case of an unforced system the solution to the Equations of Motion (EoM) can be used to set up the equations which are used to give the homogeneous solution. The homogeneous solution is what describes the transient motions of the system. The EoM can be obtained by using the displacement method for an immovable base.

$$F = m \cdot a = m \cdot \frac{dx^2}{dt^2} = m \cdot \ddot{x} \tag{1}$$

The forces acting on the mass can be found as:

$$m\ddot{x} = -F_k - F_c + F_{external} \tag{2}$$

For free vibration the external loading is neglected and the spring and damping forces can be superimposed resulting in:

$$m\ddot{x} = -c\dot{x} - kx \tag{3}$$

Rewriting the system to the left hand side results in the equations of motion for the system.

$$m\ddot{x} + c\dot{x} + kx = 0 \tag{4}$$

To obtain an equation with fewer variables the following widely known relations are used. In which ω_n is the natural frequency in rad/s and ζ is the relative damping ratio.

$$\omega_n = \sqrt{\frac{k}{m}} \tag{5}$$

$$\zeta = \frac{c}{2\sqrt{m \cdot k}} \tag{6}$$

Using the relations the equation of motion is rewritten to:

$$\ddot{x} + 2\,\zeta\omega_n\dot{x} + \omega_n^2 x = 0 \tag{7}$$

The damping reduces the eigenfrequency, therefore the eigenfrequency with damping becomes:

$$\omega_d = \omega_n\sqrt{1-\zeta^2} \tag{8}$$

The general solution to the system in equation 7 is:

$$x_{hom}\,(t) = C_1 e^{r_1 t} + C_2 e^{r_2 t} = \sum_{i=1}^{2} C_i e^{r_i t} \tag{9}$$

In which $C_1 and\ C_2$ are dependent on the initial conditions and $r_1 and\ r_2$ are given by

$$r_{1,2} = -\zeta\omega_n \pm \sqrt{\omega_n^2(\zeta^2-1)} \tag{10}$$

The solution for free vibrations is given by:

$$x_{hom}(t) = C_1 \cdot e^{-\zeta\omega_n t} \cdot e^{\sqrt{\omega_n^2(\zeta^2-1)}} + C_2 \cdot e^{-\zeta\omega_n t} \cdot e^{-\sqrt{\omega_n^2(\zeta^2-1)}} \tag{11}$$

The parameters C_1 and C_2 can be solved using the initial conditions of the system. i.e. $x(t=0) = x_0, \dot{x}(t=0) = v_0$

2.1.2 Forced Vibrations

The forced vibrations come mainly in two types, the base excitation and the direct loading. Both types will be evaluated in this section.

2.1.2.1 Base excitation

The OC motions are modelled by the dynamic system shown in Figure 2-1. The vessel is in constant motion therefore in reality the mass will be subjected to loads caused by a base excitation. The equation of motion is set up in a similar manner to the one in section 2.1.1. The base excitation $[x_b]$ is assumed harmonic resulting in:

$$x_b(t) = X_b e^{i\Omega t} \tag{12}$$

The shape of the base excitation is assumed to be sinusoidal

$$x_b(t) = x_b \cdot \sin(\Omega t) = Im\left(X_b e^{i\Omega t}\right) \tag{13}$$

Or

$$x_b(t) = X_b e^{st} for\ s = i\Omega \tag{14}$$

The equation of motion is written as:

$$m\ddot{x} = -c\dot{x} - kx + c\dot{x}_b + kx_b \tag{15}$$

The system can be rewritten to

$$m\ddot{x} + c\dot{x} + kx = c\dot{x}_b + kx_b \tag{16}$$

Using the simplification with the natural frequency and the relative damping the complete system is obtained. The same transient solution (obtained in section 2.1.1) is valid for this system. In addition to the transient solution there is the steady state part of the solution. The steady state solution is a stationary solution to the EoM. After the transient motions have damped out the steady state motions will be left. Which will be the case for a dredge vessel which will operate for several hours. The solution the steady state solution is based on the extended equations of motion.

$$\ddot{x} + 2\,\zeta\omega_n \cdot \dot{x} + \omega_n^2 \cdot x = \dot{x}_b \cdot 2\zeta\omega_n + x_b \cdot \omega_n^2 \tag{17}$$

Using the shape function $[Xe^{st}]$ due to its similarity to the base excitation is done to get a possible particular solution for which the amplitude $[X]$ can be solved using the differential equation. Using the Laplace transformation in which $s = i\Omega$. For a sine function the particular solution becomes:

$$x_p(t) = Xe^{st} \tag{18}$$

$$\dot{x}_p(t) = sXe^{st} \tag{19}$$

$$\ddot{x}_p(t) = s^2 X e^{st} \tag{20}$$

Filling this in the EoM results in

$$X(s^2 + 2\,\zeta\omega_n s + \omega_n^2)e^{st} = X_b(2\,\zeta\omega_n s + \omega_n^2)\mathrm{e}^{\mathrm{st}} \tag{21}$$

Solving the equation for X results in the amplitude for the particular solution.

$$X = X_b \cdot \frac{2\,\zeta\omega_n s + \omega_n^2}{s^2 + 2\,\zeta\omega_n s + \omega_n^2} \tag{22}$$

The particular solution for a sinusoidal excitation is:

$$x_p(t) = Im\left(X_b \cdot \frac{2\,\zeta\omega_n s + \omega_n^2}{s^2 + 2\,\zeta\omega_n s + \omega_n^2} \cdot e^{st}\right) \tag{23}$$

The complete solution to the forced vibrations issue is the homogeneous solution added to the particular solution.

$$x(t) = x_p(t) + x_{hom}(t) \tag{24}$$

$$\begin{aligned} x(t) = {} & Im\left(X_b \cdot \frac{-2\,\zeta\omega_n i\Omega + \omega_n^2}{-\Omega^2 - 2\,\zeta\omega_n i\Omega + \omega_n^2} \cdot e^{i\Omega t}\right) \\ & + C_1 \cdot e^{-\zeta\omega_n t + \sqrt{\omega_n^2(\zeta^2-1)}} + C_2 \cdot e^{-\zeta\omega_n t - \sqrt{\omega_n^2(\zeta^2-1)}} \end{aligned} \tag{25}$$

C_1 and C_2 can be found using the initial conditions. Initial conditions $x(0) = 0\ and\ \dot{x}(0) = 0$ gives $C_1 = and\ C_2 =$ However for $t \to \infty$ the homogeneous solution becomes 0 and the resulting motions are the steady state motions. The steady state motions are of interest for continuous loading.

To obtain the excitation amplitudes using the transmissibility $[H]$ of the system is a known approach to obtain the resulting amplitude. The transmissibility of the system is the ratio between the amplitude of the base excitation and the resulting motion of the mass.

$$\frac{X}{X_b} = \frac{-2\,\zeta\omega_n i\Omega + \omega_n^2}{-\Omega^2 - 2\,\zeta\omega_n i\Omega + \omega_n^2} \tag{26}$$

The amplitude of the transmissibility $[H]$ is obtained by taking the square root of the squared real and imaginary parts of the transmissibility. The phase angle $[\phi]$ is determined by taking the arctan of the imaginary part over the real part.

$$H = \sqrt{Re^2\left(\frac{X}{X_b}\right) + Im^2\left(\frac{X}{X_b}\right)} \tag{27}$$

$$\phi = \arctan\left(-\frac{Im\left(\frac{X}{X_b}\right)}{Re\left(\frac{X}{X_b}\right)}\right) \tag{28}$$

Using these relations a Bode plot for several values of the relative damping can be constructed as shown in Figure 2-2.

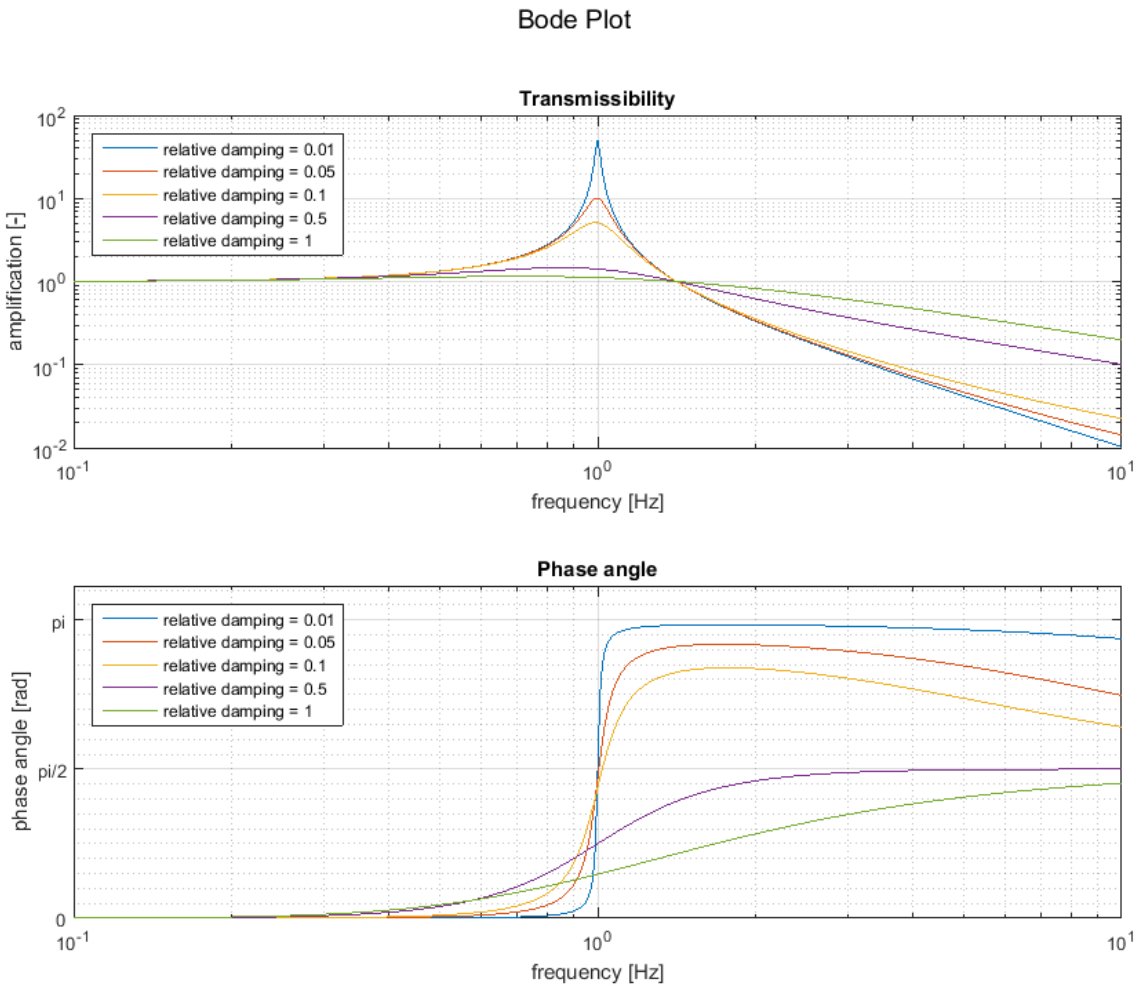

Figure 2-2, Bode plot for different relative damping values

2.1.2.2 Direct loading

When the system is directly subjected to a load, for example the wind or a person pushing against the mass the resulting displacement is different from the displacement due to the base excitation. The main difference is that the load is directly applied and is not dependent on the system properties $[c]$or $[k]$. therefore the motions caused by the direct loading are considered separately. The EoM for the directly loaded system is

$$m\ddot{x} + c\dot{x} + kx = F(t) \tag{29}$$

$$\ddot{x} + 2\zeta\omega_n\dot{x} + \omega_n^2 x = \frac{F(t)}{m} \tag{30}$$

$$F(t) = F_0 e^{i\Omega t} \tag{31}$$

The loaded system has a solution which consists of a homogeneous and a particular part. The homogenous part is identical to the one in section 2.1.1

$$x(t) = x_p + x_{hom} \tag{32}$$

The particular solution is the steady state solution for a damped system. The steady state solution is the motion pattern by which the mass is described when the homogeneous part of the solution has damped out. The solution assumes (Spijkers, 2005) that the particular solution has the same frequency and general form as the forcing function. While the frequency is the same, a phase difference can be present.

$$x_p = Xe^{i\Omega t} \tag{33}$$

$$X = \frac{F_0}{ms^2 + cs + k} = \frac{F_0}{k - m\Omega^2 - ci\Omega} \tag{34}$$

$$Amplitude = A = \sqrt{Re^2(X) + Im^2(X)} \tag{35}$$

$$Phase\ angle = \phi = \arctan\left(\frac{Im(X)}{Re(X)}\right) \tag{36}$$

$$A = \frac{\frac{F_0}{k}}{\left(\left(1 - \left(\frac{\Omega}{\omega_n}\right)^2\right)^2 + (2\zeta\Omega\omega_n)^2\right)^{\frac{1}{2}}} \tag{37}$$

$$\phi = \tan^{-1}\left(\frac{2\zeta\frac{\Omega}{\omega_n}}{1 - \left(\frac{\Omega}{\omega_n}\right)^2}\right) \tag{38}$$

The base excitation system is extremely similar, the only difference is:

$$F_0 = k * x_b \rightarrow \frac{F_0}{k} = x_b \tag{39}$$

Solving the system gives a response function. The response function divided by the amplitude of the load or the base excitation gives a function for the dynamic amplification factor. The DAF is a factor by which the steady state amplitude is magnified depending on the forcing frequency [Ω] and the damping ratio [ζ]

2.1.2.3 Conclusion

The limits for the direct load in $\frac{F_0}{X}$ for $\Omega \to 0$ is $\frac{1}{k}$ and for $\Omega \to \infty$ the slope of the line goes to $[10^{-2}]$, in the logarithmic domain $[-2]$. this means that the lower the stiffness is, the larger the excitation will be due to direct loading. The isolation of the higher frequencies is very good.

The upper limits for the base excitation are dependent on the damping value. The lower limits are independent for the damping value and $\left[\frac{X}{X_b}\right]$ for $\Omega \to 0$ goes to 1. The upper limit for $\zeta \approx 0 \; and \; \Omega \to \infty$ results in the slope of the line going to $[10^{-2}]$, he upper limit for $\zeta \geq 1 \; and \; \Omega \to \infty$ results in the slope of the line going to $[10^{-1}]$. The implications of this are that the less damping is present the more effective the vibrations of the higher frequencies are isolated. However for lower damping value the amplification of vibrations is more severe.

2.1.3 Gravitational deflection

Using a dynamic system in the vertical direction adds gravity to the loading conditions. The gravity on the mass is a constant load and results in a constant steady state deflection δ for which the spring force equals the gravity load. The gravity load can be put into the EoM leading to an extended system.

$$m\ddot{x} + c\dot{x} + kx = F_z \tag{40}$$

$$F_z = m \cdot g \tag{41}$$

The particular solution to this system can be found using the form

$$x_p(t) = \delta$$

$$\dot{x}_p(t) = 0 \tag{42}$$

$$0 + 0 + \; k \cdot \delta \; = F_z$$

Resulting in the steady state deflection of

$$\delta = \frac{m}{k} \cdot g = \frac{g}{\omega_n^2} \tag{43}$$

The gravity deflection is therefore only dependent on the eigenfrequency of the system. In Figure 2-3 the static deflection curve for earth is plotted vs eigenfrequency. This curve is valid for all linear mass spring systems subjected to gravitational force.

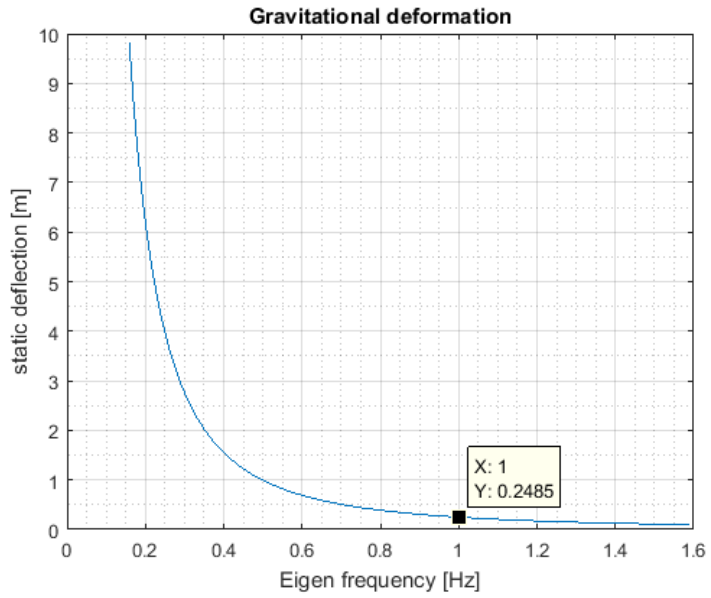

Figure 2-3, static deflection vs eigenfrequency

2.1.4 Additional degrees of freedom

Addition of more degrees of freedom to the system results in the expansion of the equations of motion into a system of equations of motion as shown in equation 44. in which M, C and K are matrices and F is a vector.

$$M\ddot{x} + C\dot{x} + Kx = F \tag{44}$$

An example is shown using an undamped 2D system which has two degrees of freedom (DoF) in translation and one DoF in rotation.

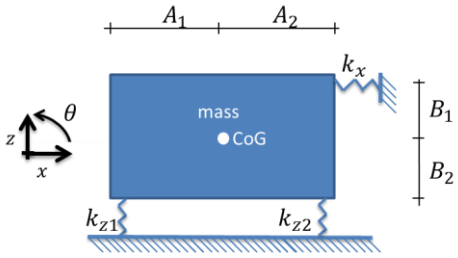

Figure 2-4, 3DoF system schematic

The equations of motion are

$$m\ddot{x} = -k_x \cdot x - \theta \cdot B_1 \cdot k_x \tag{45}$$

$$m\ddot{z} = -k_{z1} \cdot z - k_{z2} \cdot z - A_1 \cdot k_{z1} \cdot \theta + A_2 \cdot k_{z2} \cdot \theta \tag{46}$$

$$J\ddot{\theta} = -\theta \cdot A_1^2 \cdot k_{z1} - \theta \cdot A_2^2 \cdot k_{z2} - \theta \cdot B_1^2 \cdot k_x - A_1 \cdot z \cdot k_{z1} + A_2 \cdot z \cdot k_{z2} + B_1 \cdot k_x \cdot x \tag{47}$$

The system of equations can be rewritten as

$$M\begin{bmatrix}\ddot{x}\\ \ddot{z}\\ \ddot{\theta}\end{bmatrix} + K\begin{bmatrix}x\\ z\\ \theta\end{bmatrix} = F \tag{48}$$

$$\begin{bmatrix}m & 0 & 0\\ 0 & m & 0\\ 0 & 0 & J\end{bmatrix} \cdot \begin{bmatrix}\ddot{x}\\ \ddot{z}\\ \ddot{\theta}\end{bmatrix} + \begin{bmatrix}k_x & 0 & B_1 \cdot k_x\\ 0 & k_{z1} + k_{z2} & A_1 \cdot k_{z1} - A_2 \cdot k_{z2}\\ B_1 \cdot k_x & A_1 \cdot k_{z1} - A_2 \cdot k_{z2} & A_1^2 \cdot k_{z1} + A_2^2 \cdot k_{z2} + B_1^2 \cdot k_x\end{bmatrix} \cdot \begin{bmatrix}x\\ z\\ \theta\end{bmatrix} = \begin{bmatrix}F_x\\ F_z\\ M\end{bmatrix} \tag{49}$$

Additional degrees of freedom increase the complexity of the system but the principles do not change. The complex notation of the general solution is used as the solution of the system.

$$x(t) = \sum_{i}^{2N} X_i \, e^{s_i t} \tag{50}$$

The general solution is filed into the system of equations and is used as the homogeneous solution. This results in the characteristic equation for the eigenvalues and eigenmodes.

$$\left(s_i^2 \cdot M + K\right)X_i e^{s_i t} = 0 \tag{51}$$

Since the exponential cannot be zero (or the result would be a trivial solution) the resulting equation for determining the eigenfrequencies

$$\left(s_i^2 \cdot M + K\right)X_i = 0 \tag{52}$$

Resulting in the characteristic equation

$$\det\left(s_i^2 \cdot M + K\right) = 0 \tag{53}$$

The eigenvalues are the positive roots of the characteristic equation. In the previous system there are three different eigenvalues.

$$s_1, s_2, s_3 \tag{54}$$

To each natural frequency belongs an eigenmode. The eigenmodes are displacements in different directions given by the the eigenvectors to the system for each eigenfrequency. By inserting s_1, s_2, s_3 in equation 52, resulting in three vectors X_1, X_2, X_3 the vectors are the eigenvectors. Each eigenvector represents the coupled displacement of the system of all degrees of freedom relative to each other. These motions are called the eigenmodes. When the system is excited in with a frequency near one of the eigenfrequencies the motions of the system with respect to the other degrees of freedom is proportional to the eigenmode that corresponds to the eigenfrequency. Combination of the eigenvectors gives the eigenmatrix

$$E = [X_1\ X_2\ X_3] \tag{55}$$

The eigenmatrix can be used to shift the system into the modal regime. This reduces the complexity of the calculations but results in modal movement, this movement is not corresponding to the physical reality.

2.1.5 Non-linear vibrations

A real spring is not linear, the stiffness depends on the amplitude of excitations. Some springs become less stiff, called softening of the spring, while some springs become stiffer, called hardening of the spring. The amount of hardening or stiffening determines the linearity of the spring. Most springs have only a small amount of non-linearity in the design area and therefore the linear approximation can be considered as accurate enough in most practical cases.

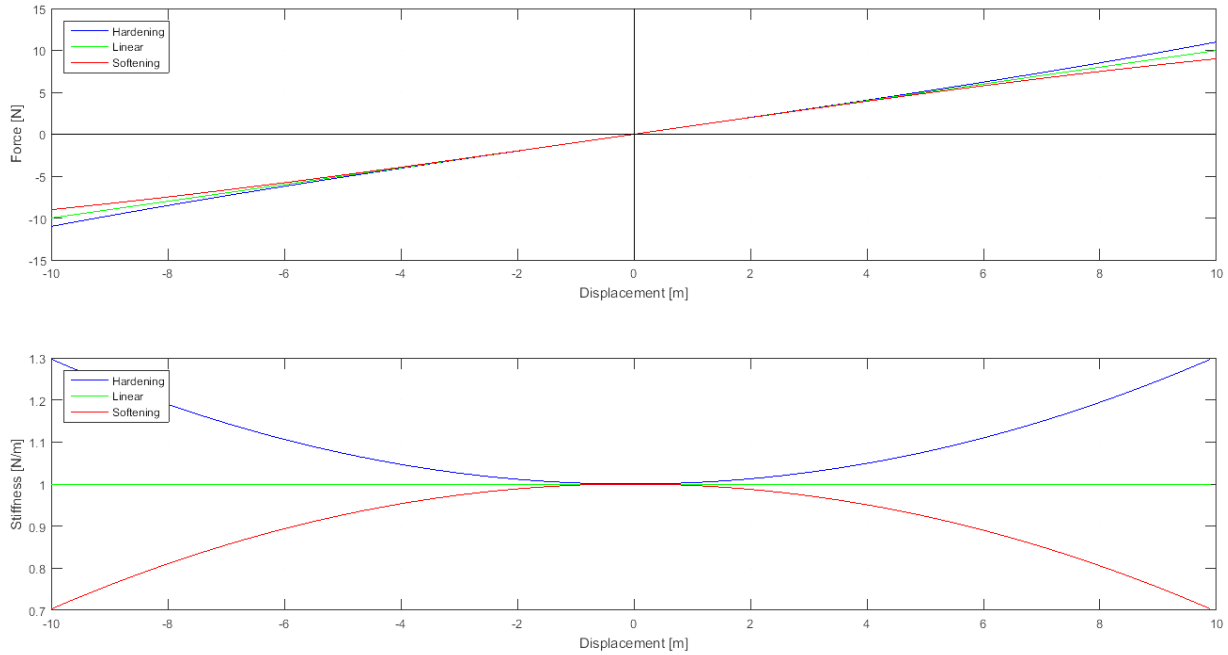

Figure 2-5, typical force-displacement and stiffness-displacement curve for three types of physical springs

In case of a non-linear spring there is no single transfer function(TF), the TF becomes dependent on the amplitude of the force.

The non-linear system of equations of motion is based on the forces acting on the system and is obtained via the same route as described in section 2.1.2. The result is given in equation 56.

$$m\ddot{x} = F_c(\dot{x}, \dot{x}_b) + F_k(x, x_b) + F_{external}(t) \tag{56}$$

In this system x is the displacement of the mass in an absolute system of reference. The parameter $x_b(t)$ is a time dependent prescribed displacement of the base. In this system F_k is the force exerted through the spring and F_c force exerted by the damping mechanism.

The system does not possess a clearly defined transmissibility. Different amplitudes have different transmissibility curves. The transmissibility for a softening, linear and stiffening spring is given in Figure 2-6. These curves are valid for systems without damping. Systems which are highly non-linear will resemble the softening and stiffening curves and the more linear systems will resemble the linear curve. When damping is introduced the maxima will no longer be infinite but will show a certain defined value.

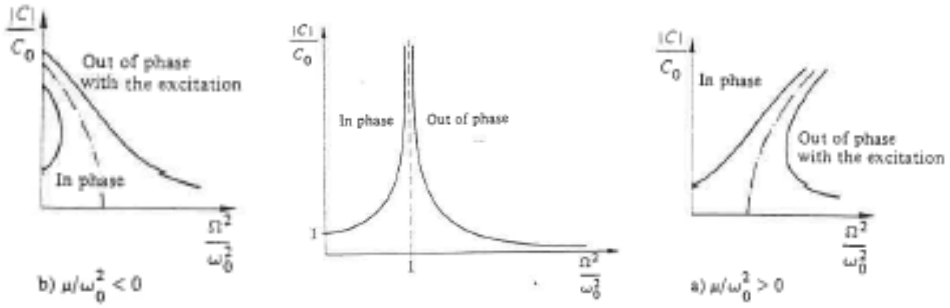

Figure 2-6, Softening, linear and stiffening transmissibility (Meijers, 1996)

2.2 Vibration isolation theory

Vibrations are motions of an object around an equilibrium point. The motions can be induced by an imposed displacement or a load. Vibration isolation is the decoupling of an object from the source of vibration. All vertical vibrations isolation systems have two main functions which can be split or combined depending on the manner of implementation. The functions are loadbearing (or gravity compensation) and payload position control. Horizontal vibration isolation is largely unaffected by gravitational loads and therefore exempt from load bearing.

Two methods of vibration isolation are, passive and active isolation. Active isolation utilises an active control loop and actuators to reduce the vibrations. Aside from completely active systems there are several kinds of passive-active combinations. However all of these require actuators and control loops. In this thesis the use of active vibration isolation is prohibited due to the higher costs.

2.2.1 Passive vibration isolation

Passive isolation refers to the process of isolation without any power input and relies on the mechanical properties of the isolators to reduce vibrations. Examples of passive isolation are systems are: the rubber pads underneath a diesel engine, the tuned mass damper in the Taipei tower or the base isolators underneath buildings in earthquake prone areas. All these systems contain mass spring and damping elements. Passive vibration isolation is the tactical choosing of the system properties relative to the excitation sources of the system to reduce the vibrations of the system.

There are two types of loads that can affect the system shown in Figure 2-1. One type of load is the external load and the other is a base excitation. The effects of these loads on the system are different. The effect of a direct loading on the amplitude of vibrations is called compliance, whereas the effect of a base excitation is called transmissibility. In the frequency domain on double logarithmic axes there are two clear asymptotes present. These asymptotes are shown in Figure 2-7. The asymptotes are for high frequency and for low frequency. The low frequency asymptote goes to $\frac{1}{k}$ for the compliance and 1 for transmissibility. The high frequency asymptote has a slope of -2 in an undamped case and -1 in a more heavily damped case for both the transmissibility and compliance. The slope indicates a larger decay in amplitude for higher frequency vibrations. The resonance peaks and amplification zone are not displayed in these graphs since the goal is vibration reduction.

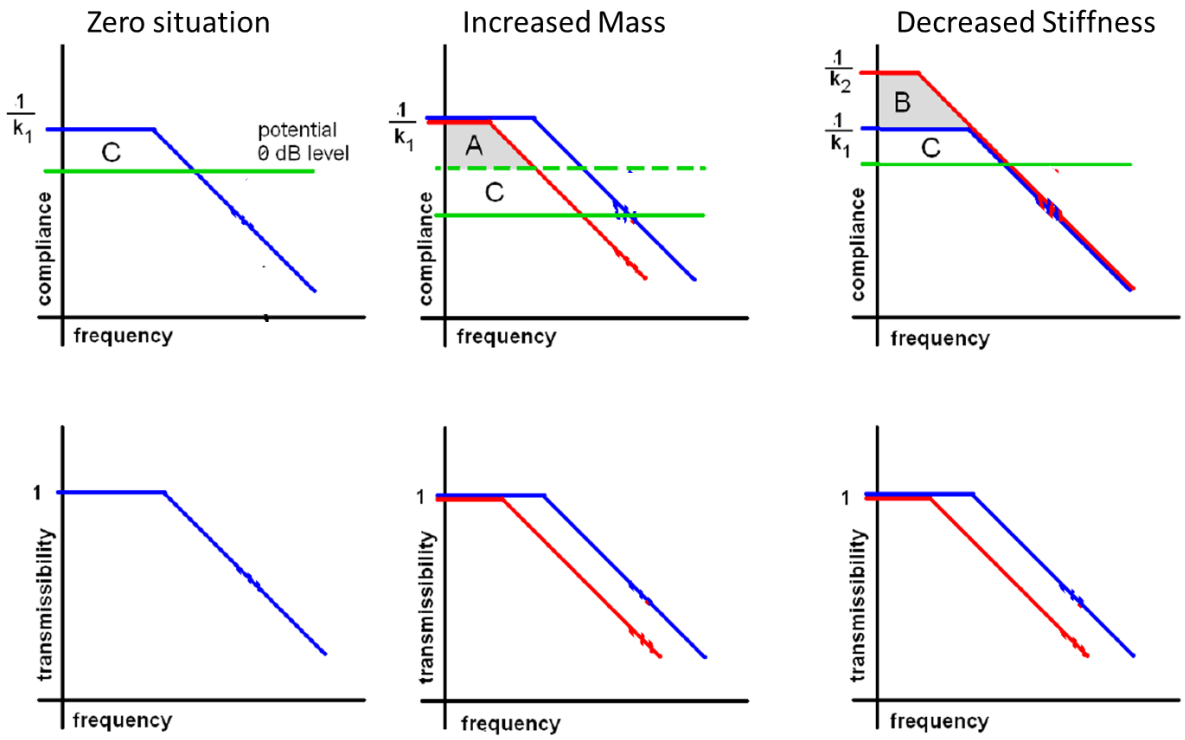

Figure 2-7, Effects of changes to mass and stiffness adapted from (Los, 2009)

In Figure 2-7 the difference between transmissibility and compliance is illustrated. The effects of changes in mass and stiffness are the same for the transmissibility however the changes for compliance are different. When reducing the eigenfrequency of the system the transmissibility shifts to the lower frequencies. When doing the same and looking at the effects on compliance, the choice whether to reduce the eigenfrequency by increasing the mass or by decreasing the stiffness has different effects. When increasing the mass the system becomes less susceptible to direct loads. When decreasing the stiffness the system becomes more susceptible to direct loading. when the compliance becomes too great, a wind load or someone pushing against the object can have the consequence of very large deflections. These effects will have to be monitored when designing such a system.

2.3 Conclusions

The result of the literature study is the theory that can be used for the rest of the thesis and the modelling phase. The reduction coefficient for the lightly damped system is of the order 10^{-2} and the reduction coefficient for more heavily damped systems is of the order 10^{-1}. Gravitational deflection is no issue for systems with eigenfrequency above $2Hz$. For the lower frequencies however the gravitational deflection has to be taken into account when designing such a system. When the system has an eigenfrequency of $1Hz$ the deflection is $250mm$.

When considering systems with multiple degrees of freedom systems, the effects of the coupling terms have to be taken into account. The translation directions can be directly affected by the stiffness and damping coefficients, the rotational directions can be affected by both the stiffness and damping parameters as well as changing the geometrical positions of the isolators.

Non-linear systems can require a change in mind-set from the linear equations which is very large. There are no available analytical solutions to these system. In the linear case the choice for the relative or the absolute displacement is not that important for non-linear systems the wrong choice results in a wrong model.

3 Inventory

This chapter discusses the results and findings regarding the IHC materials, vessels and the practical issues. This is done to provide the reader with more intimate knowledge regarding the systems present on a CSD and the behaviour of the OC- vessel system. In order to create a dynamic analysis of the beaver dredgers, the resonance and possible solutions directions have to be determined. Therefore in section 3.1 a case study is done for a typical CSD with vibration isolation problems. In section 3.2 the cause for the resonance is determined and the possible solutions for the problem are discussed. At the end of this chapter a solution to continue the research with is chosen.

3.1 Case study

In this section a case will be studied to fully understand the problem. This is necessary to be able to provide IHC with a workable solution.

- Provide a connection between theory and practice
- Provide one solution to focus further investigation

The vessel of choice for the case study is the Shanti Sagar XVI. A Cutter suction dredger built in 2011 by IHC. The SSXVI is a vessel for which a large warranty claim was issued. The warranty claim resulted in a large amount of data for study. Aside from the SSXVI there is a similar CSD built by IHC, the Quibian I. This vessel has experienced the same issues and has some additional data available for study.

3.1.1 Introduction to the SSXVI

The Shanti Sagar XVI is a Beaver type CSD. A CSD is a type of dredge vessel which uses a rotating cutter head to physically break the seabed into smaller pieces. The pieces are transported hydraulically through the vessel. A CSD has no storage capacity and relies either on a barge moored alongside or a pipeline to a discharge location. The CSD is propelled by spud piles combined with anchor lines to swivel the vessel around. The Hull is usually rectangular or pontoon shaped since the vessels operate in mild waves. The vessel is equipped with a dredge ladder and a cutter head as dredging equipment. On board there are various pumps and machines to allow for operations. On top of the vessel there is an Accommodation Cabin (AC) and Operator Cabin (OC). These are set separate from the main hull and isolated by a number of rubber vibration isolation profiles.

Figure 3-1, Shanti Sagar XVI launch at IHC slipway (Royal IHC, MTI)

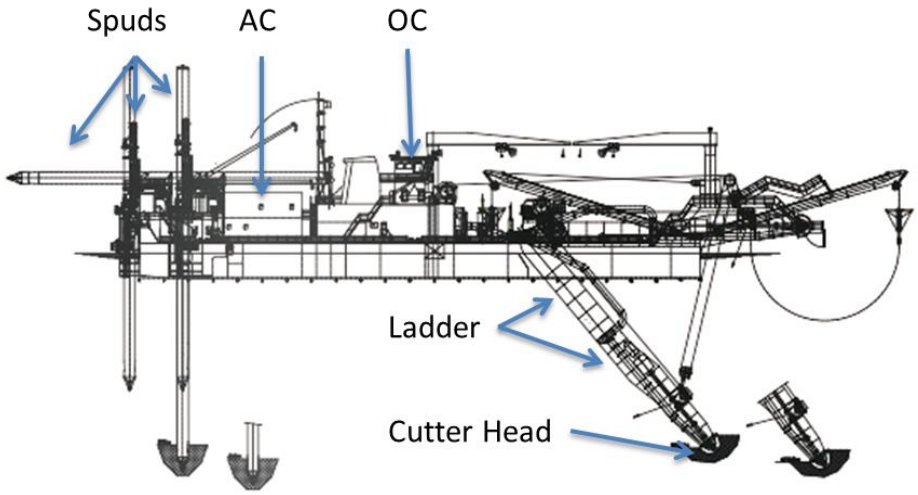

Figure 3-2, Beaver 9029 Schematic (Royal IHC, MTI)

The OC and the AC have experienced large vibrations during operations. The crew of the vessel attempted to dampen the vibrations by applying ratchet straps to the top of the OC. The straps limited the motions of the OC insufficiently. Complaints regarding the sleeping and working environment were issued. It was reported that computers and monitors were vibrating and falling down and that working conditions were particularly poor. The complaints resulted in a warranty claim which resulted in action from IHC.

Table 1, Shanti Sagar XVI vessel properties

Length (OA):	104 m
Width:	18.6 m
Depth:	5 m
Cutter power:	1500 kW
Total power:	13000 kW
Delivery diameter:	900 m
Dredging depth:	29 m
Suction pipe diameter:	0.9 m

3.1.2 The warranty claim

IHC personnel was sent to the vessel due to the warranty claim. Interviews were conducted, with the personnel of the client. The experience of the crew is that the problematic vibrations only occur when dredging very hard soils. The reports indicate that the motions of the OC is a combination of heave and pitch. To obtain a more complete picture, measurements were performed. The measurements determined de individual system vibrations and an overall Operational Deflection Shape (ODS). In Figure 3-3 and Figure 3-4, the velocity spectra of the motions of the four corners of the OC and four points directly below the OC on the Vessel are given for a cutter speed of 40 rpm. The measurements were performed with a handheld measurement device, the device automatically gives the spectra in [mm/s rms].

Several observations can be made from the graph. There is an increase in the amplitude of the velocity between the Vessel and the OC in the heave direction. The increase in amplitude for the sway direction in negligible. The increase in velocity amplitude for the surge direction depends on the point measured. The shape of the vibration spectra for the OC are smoother than the spectra for the points on the vessel, this indicates the shedding of vibrations to different frequencies. The shedding of vibrations into different frequencies can be due to the non-linearity of the rubber suspension.

The amplification in heave direction points towards a resonance and is most likely due to the rubber supports. The relative scale of the different directional components is shown in Figure 3-4 (right).

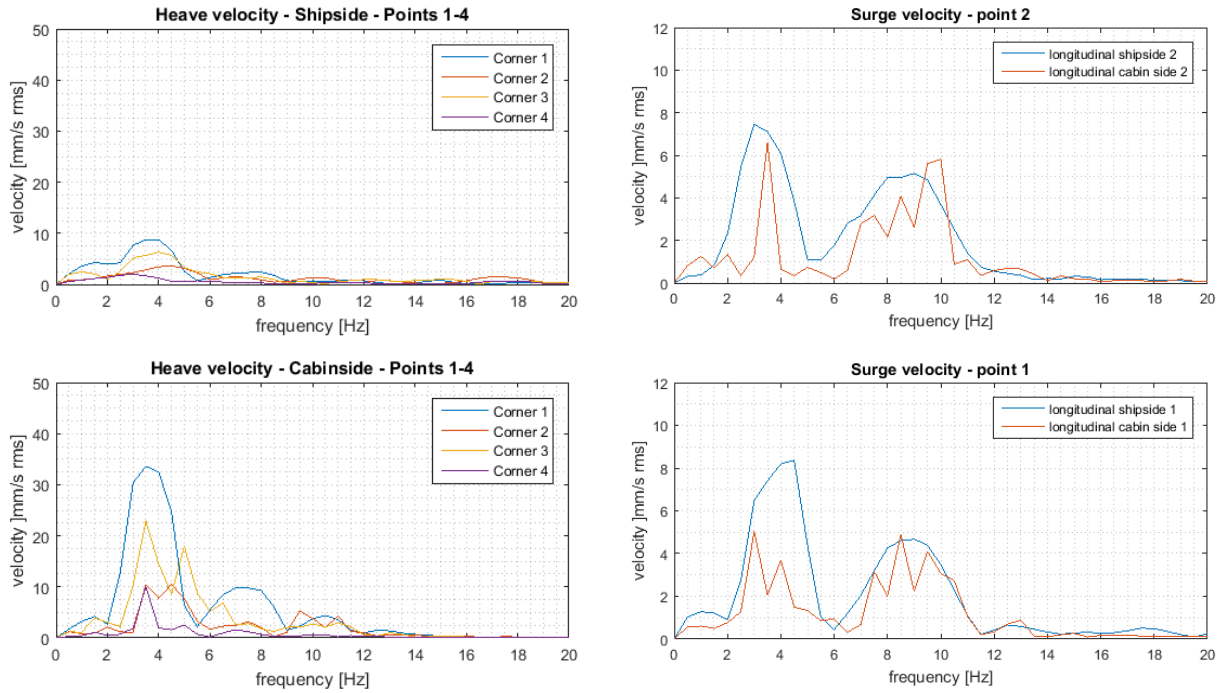

Figure 3-3, heave (left) and surge (right) velocities [mm/s rms] for 40 rpm cutter speed

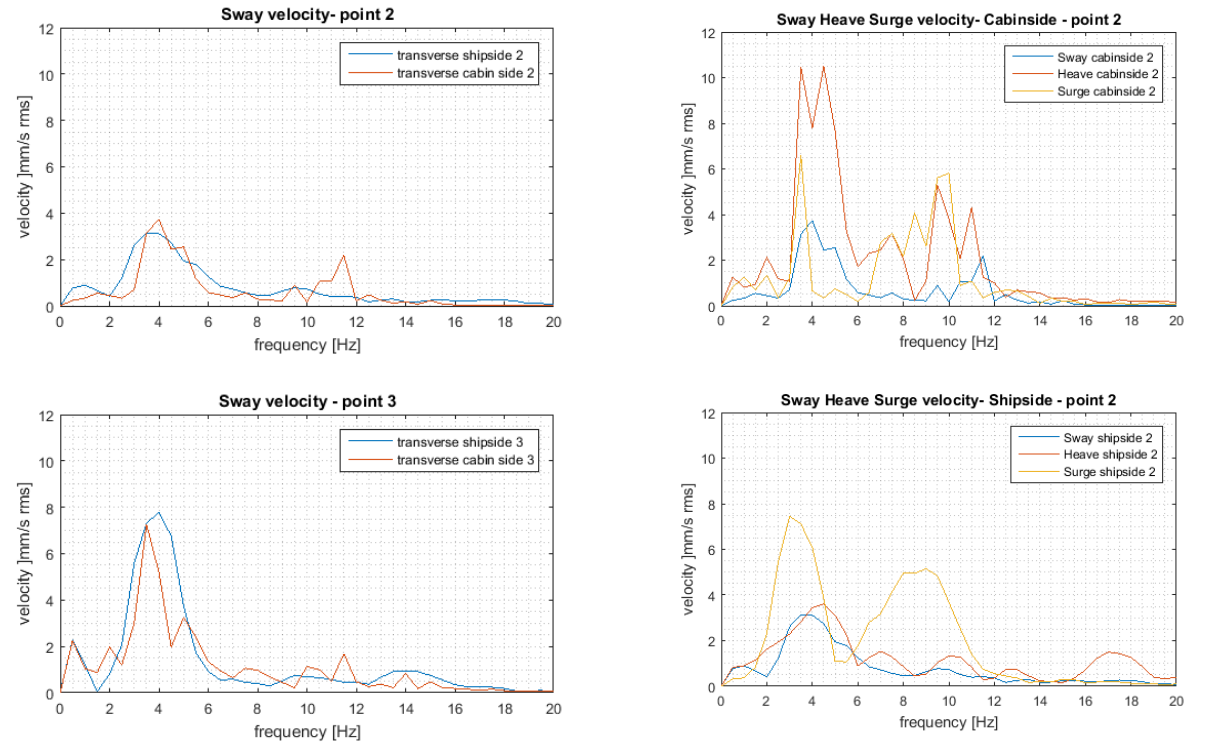

Figure 3-4, sway (left) and combination (right) velocity [mm/s rms] for 40 rpm cutter speed

3.1.3 The IHC Solution

A quick solution was essential since the vessel was already in operation. In this case the source vibrations were not deemed excessive. Therefore the resonance could be eliminated by replacing the rubber dampers with steel supports, in essence welding the OC directly to the deck. The solution eliminated the resonance and a large part of the inconvenience. However higher frequency vibrations became more prominent in the OC and AC. The resulting spectrum can be seen in Figure 3-5. Visible are the sharp peaks in the spectrum, indicating narrow band near sinusoidal vibrations. The solution allowed the client to resume working with minimal delay and it was to the satisfaction of the client. Originally the system with rubber isolation was designed to reduce the vibrations and increase comfort in the OC. The currently installed welded system is not isolating the vibrations anymore therefore the welded solution is overall considered suboptimal and a new solution is required.

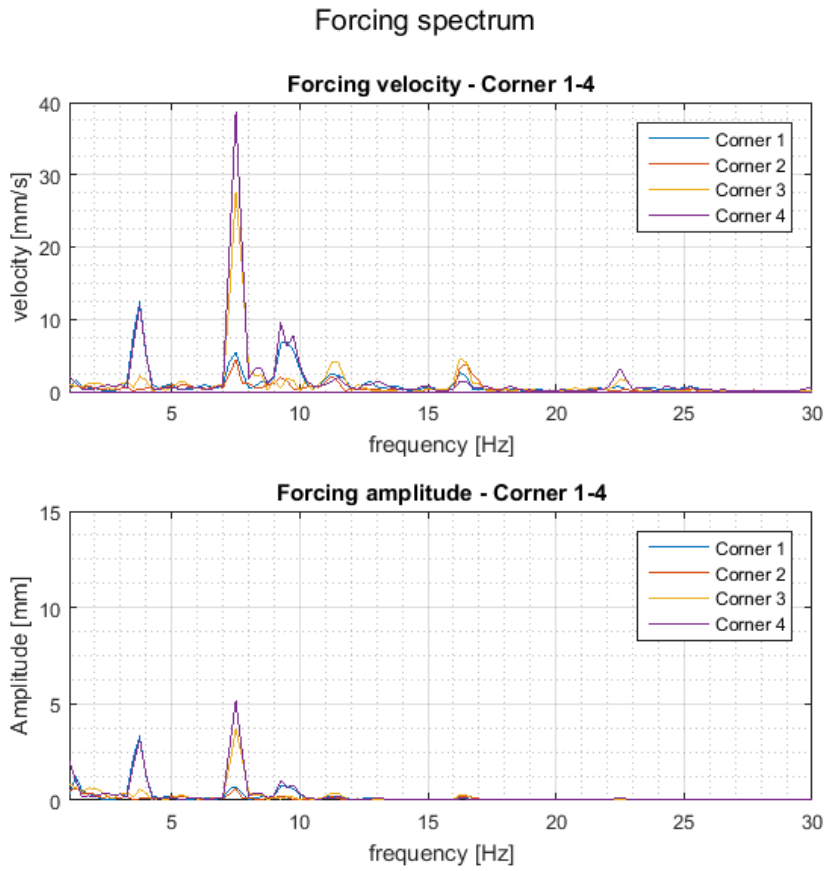

Figure 3-5, Heave velocity and amplitude for SSXVI steel on steel

3.1.4 Fresh look

A fresh look with the same data and increased dynamics knowledge may shed new light on the issue. In the previous section it was shown that the vibrations at low frequencies, were amplified indicating that the dynamic system was operating in the amplification zone. With a properly calibrated system, however the vibrations can be designed to be minimised. The current vibrations are detrimental to the working conditions and have to be reduced.

The isolation of vibrations can be focussed on several locations at the vessel. The vibrations present in Figure 3-5 originate from different sources. The sources are the cutter head, dredge pumps and genset/engine of which the cutter head is the main source. To reduce the amplitudes of the vibrations in the OC and AC, several approaches might be feasible. Source isolation is the isolation of the vibrations at the source of the vibration path. To properly isolate the source, all sources need to be considered. In this case the engine and the pumps can be flexibly mounted to isolate the vibrations, the cutter head might be isolated by mounting the ladder flexibly and the pipelines alongside the dredge pumps will have to be flexibly mounted. Instead of all these measures, application of target isolation would cause the OC and AC to be isolated at the interface of the two substructures i.e. cabins and vessel. It is deemed most effective to create a well-functioning vibration isolation system at the base of the OC and AC. The type of vibration isolation to be applied will be determined in section 3.3.

3.1.4.1 IHC design process

The original vibration isolation was designed for the isolation of machine vibrations. The machine vibrations are the vibrations that show up during the standardised harbour testing all of the CSDs go through before delivered to the client. The cutter frequencies do not show up in the results of these harbour tests. The harbour tests do not include cutting of material. The results of these tests combined with the lack of complaints regarding the suspension lead the design team to focus on more critical aspects for the design of this vessel. In other CSDs this appears to be the correct approach, the lack of complaints is attributed to the smoother excitation pattern for the cutting of softer soil types in which the CSDs normally operate.

IHC did not revise the design procedure for newer cutters since the old procedure appeared to be functioning. when cutters were designed for harder soils the procedure was to simply order the suspension systems at a manufacturer. The manufacturer received the cabin specifications but no excitation spectrum or other information regarding the forcing of the system. The resulting mode shapes and eigenfrequencies were delivered (Table 2 and Table 3) to IHC and the suspension system was approved without anyone suspicious of any problems.

A comparison of natural frequencies in Table 2 with the forcing spectrum shown in Figure 3-5 is revealing that at around 4 Hz and 8 Hz there is energy in the forcing spectrum close to the eigenfrequencies of the system. Thus special attention is required in the design of the system.

Table 2, Natural frequencies (Royal IHC, MTI)

	f1 Longitudinal	f2 Lateral	f3 Vertical	f4 Rolling	f5 Pitching	f6 Yawing
[Hz]	4,44	6,67	8,03	14,60	14,48	11,89
[1/min]	266,54	400,05	481,76	875,70	868,65	713,36

The Natural frequencies given are linked to a main motion direction of the system. The main motions are coupled using the cross terms in the modal shapes.

Table 3, Mode Shapes (Royal IHC, MTI)

	x [mm]	y [mm]	z [mm]	roll [rads]	pitch [rads]	yaw [rads]
Mode No 1	1,000E+00	0,000E+00	-5,434E-02	0,000E+00	4,132E-04	0,000E+00
Mode No 2	0,000E+00	1,000E+00	0,000E+00	-2,569E-04	0,000E+00	6,512E-06
Mode No 3	4,655E-02	0,000E+00	1,000E+00	0,000E+00	6,103E-06	0,000E+00
Mode No 4	0,000E+00	1,244E+00	0,000E+00	1,000E-03	0,000E+00	-5,255E-05
Mode No 5	-1,275E+00	0,000E+00	4,048E-02	0,000E+00	1,000E-03	0,000E+00
Mode No 6	0,000E+00	3,403E-02	0,000E+00	6,110E-05	0,000E+00	1,000E-03

Combination of Table 2 and Table 3 shows that the eigenfrequency of the third mode of vibration closely overlaps with a peak in the excitation spectrum. These properties indicate that amplification of the vibrations of the OC was inevitable. The new design needs a closer look at the exact forcing mechanisms in combination with the system characteristics.

3.1.4.2 Ideal design conditions

During the interviews certain properties were highlighted for the proper design of the vibration isolation system for CSDs.

- the system should support the OC in 6DOF and preferably not be over constrained.
- the system has to reduce the excitation vibrations
- the system has to be able to survive seawater conditions
- the system should be cost effective

3.2 Identification of driving frequencies

The frequencies at which a vessel is excited is one of the main drivers for undesired behaviour and can be altered in some cases to change the behaviour.

A Cutter Suction Dredger is a special case of a working ship, along with the vibration drivers on regular ships, the CSD has a rotating cutter head. A ship in general is subjected to wave and current loads. Waves and tides are typically low frequency vibrations (about 0.1-0.5 Hz). The other source of vibrations on a ship are the large and heavy machinery on board which can cause severe vibrations. These vibrations are usually of higher frequencies (about 10Hz). In addition to these vibrations, the CSD has a cutter wheel, which operates in the mid-frequency range (about 2-4 Hz).

3.2.1 Wave induced motions

The influence of the waves on the vessel is dependent on the sea state and the Response Amplitude Operators (RAOs). Similar to a vibration with a transfer function and an output, the output or vessel motion is the result of the sea state amplitude times the RAO for a certain frequency in a linear system.

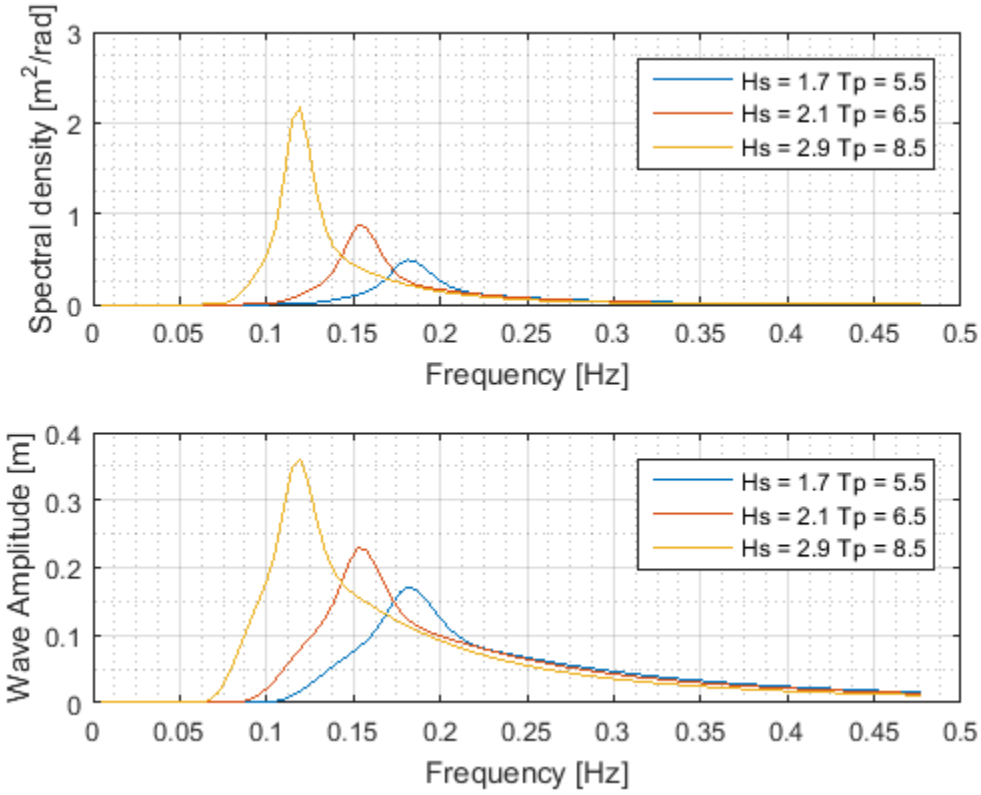

Figure 3-6, JONSWAP amplitude spectrum for governing wave parameters

In the North sea, the sea state can be characterised with the JONSWAP spectrum. The spectrum gives an indication of the different waves that are caused by the wind. The characteristic of the sea state changes with the length of the fetch over the water. A general indication on the wave height can be found from the energy spectrum assuming that the sea state consists of a summation of sinusoidal waves. Using the

simplified properties of the energy spectrum the wave height and wave amplitude are obtained. (Stewart, 2006)

$$S(\omega)d\omega = \frac{1}{2}\zeta^2 \tag{57}$$

The resulting wave amplitude spectra can be used as input for the vessel motions. These motions are coupled to the sea state by the Response Amplitude Operators (RAOs). The spectra to be used are shown in Figure 3-6, the spectra are based on three significant wave heights and wave periods which are significant in the north sea.

3.2.1.1 RAO

The Response Amplitude Operators are similar to the Transfer Function of a dynamic system. The RAO times the input is what gives the output of the system, in this case the vessel motion. The RAOs are dependent on the geometry and vary for different vessels. The RAOs belonging to the Beaver 90 are used for this study. In Figure 3-7 the RAOs of the Beaver 90 are shown for different headings. The 1 degree waves are stern incoming waves and the 180 degree waves are bow incoming waves. The 90 degree waves are incoming from portside.

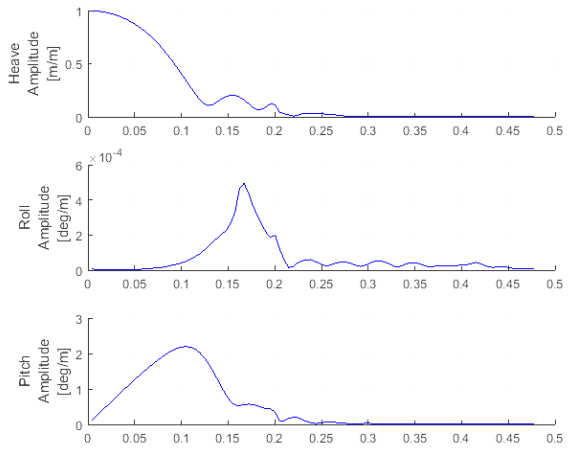

Figure 3-7, Beaver 90 - 180 deg wave direction [Hz]

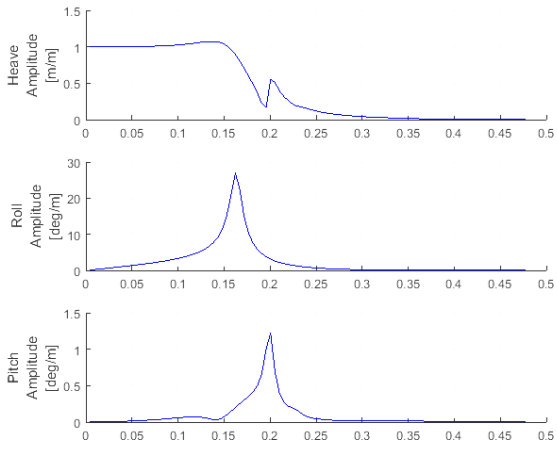

Figure 3-8, Beaver 90 - 90 deg wave direction [Hz]

The wave frequencies to which the vessel is susceptible are: 0.17 Hz roll and 0.12 Hz Pitch. For these frequencies the wave amplitude is amplified, the other frequencies are reduced. The final motions are the combination of the RAOs and the Wave Amplitude spectrum.

3.2.2 Vessel motion spectrum

The combination of the wave spectra for different fetches and the Vessel RAOs result in the excitation motions of the vessel. The motions are plotted for the response to different spectra of the waves, the Surge, Sway, Heave, Roll, Pitch and Yaw motions are plotted for each direction, different directions are plotted in individual plots. The results indicate that there are no significant motions over 0.3 Hz. Below 0.3Hz, there are some significant heave motions and some pitch.

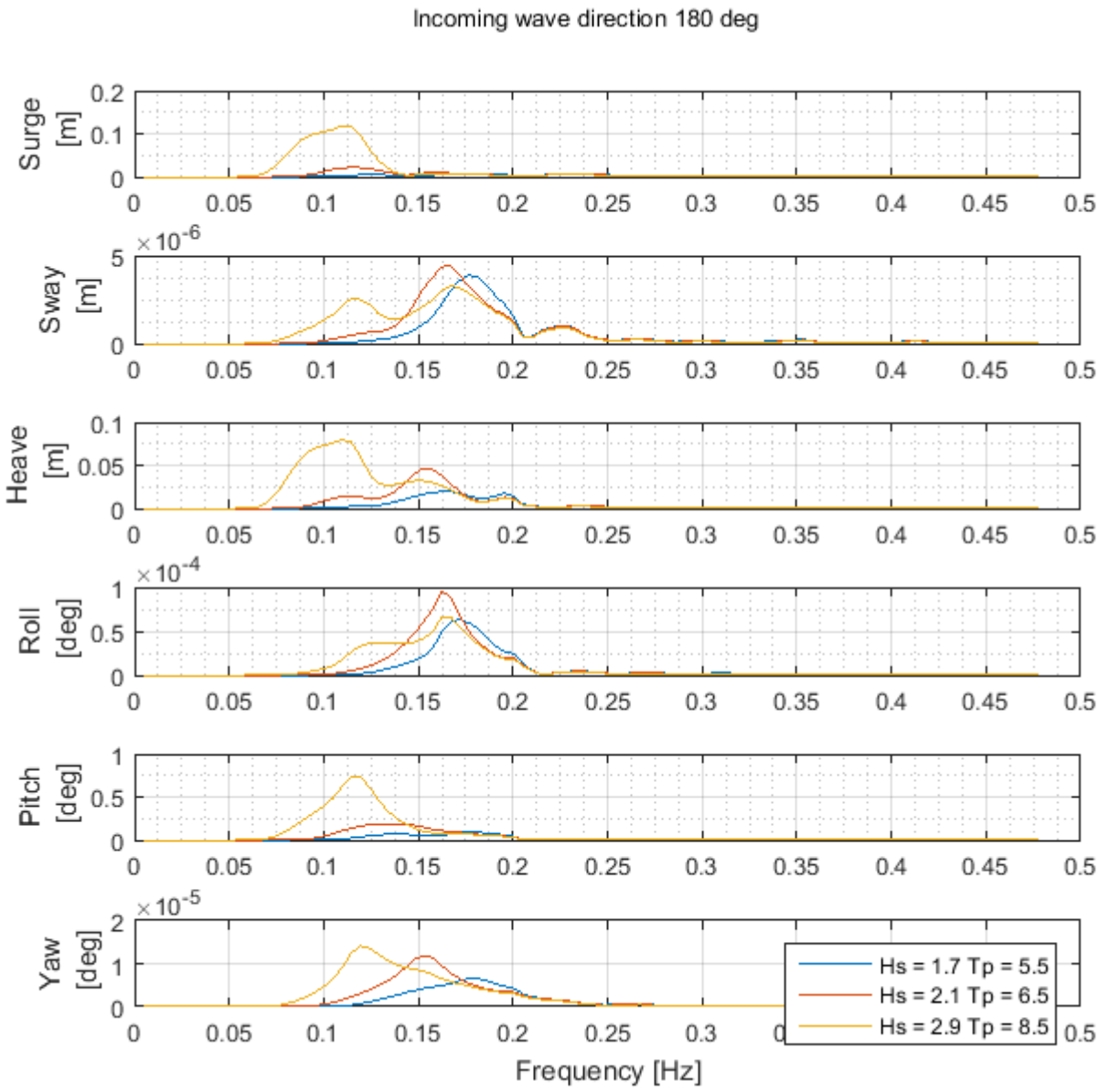

Figure 3-9, Vessel motion spectra bow waves

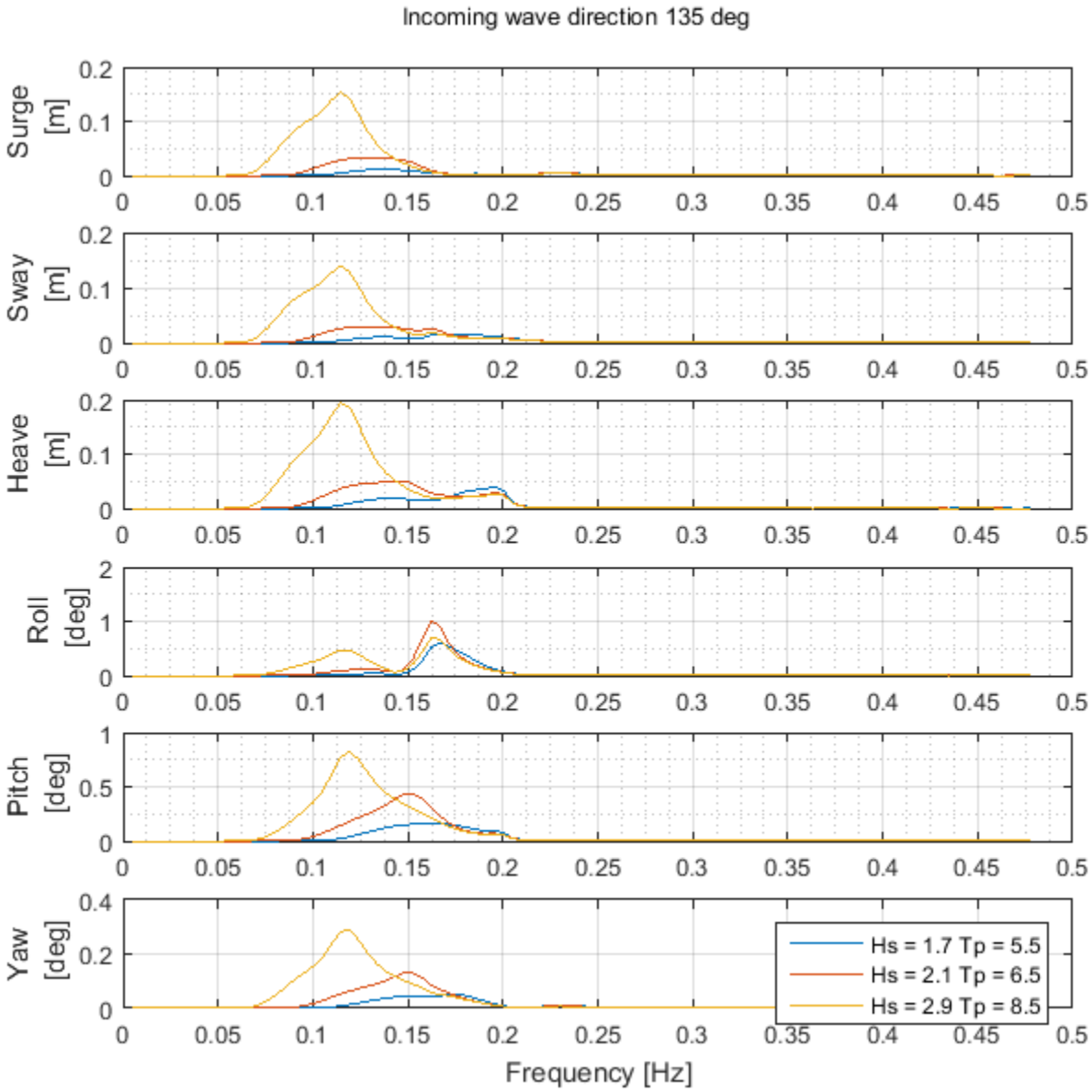

Figure 3-10, Vessel motion spectra cross waves

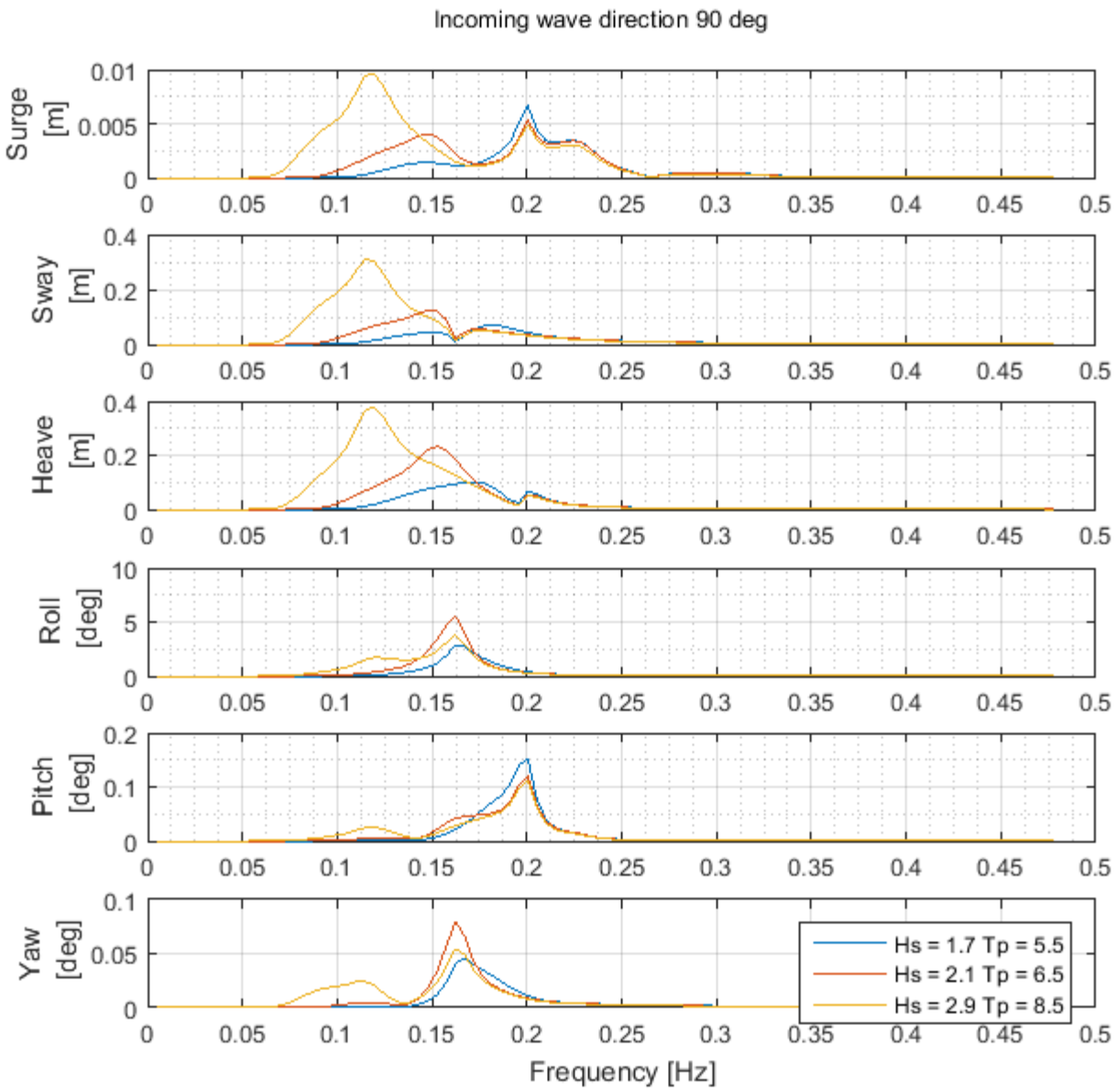

Figure 3-11, Vessel motion spectra side waves

3.2.2.1 Wave vessel Conclusions

The original design of the SSXVI suspension was not optimal for the isolation of the cutter frequencies. The waves only have limited effect on the motions of the vessel in the frequencies $> 0.3Hz$ through the RAO properties of the vessel.

3.2.3 Cutter Motions

The cutter head and the vibrations associated with that are inherent in a CSD vessel. the cutter vibrations on the vessel can be quite severe and need to be examined.

Depending on the hardness of the soil and the available power, the rotational speed of the cutter varies. A dredge master will usually try to rotate as fast as possible to maximize the production. The variation is between approximately 20 and 40 rpm or 1/3 Hz and 2/3 Hz . These frequencies are the N=1 frequencies or base frequencies. Base frequency will only appear in a spectrum when there is a misalignment issue or some other issue. The frequency for which there are larger amplitudes is the blade passing frequency.

Figure 3-12, Typical Cutter head (Royal IHC, MTI)

The blade passing frequency is dependent on the number of blades that are on the cutter head and the rotational speed of the cutter head. A typical cutter head has six blades with a number of teeth attached. There are cutter heads with a different number of blades (like the Lancelot and the Excalibur) with more blades and some smaller cutters have less blades per head however by far the most have the six blades. The blade passing frequency is in that case six times the rotational frequency or N=6. Resulting in the cutting frequencies being 2 to 4 Hz . The amplitude of these motions are completely dependent on the cutter teeth and the soil type.

3.2.4 Machine Motions

The main driving machines are: the dredge pumps, the e-motors and the diesel engine. The submerged dredge pump rotates at 216rpm or 3.6 Hz, with three blades the blade passing frequency is 10.8 Hz. The N=1 frequency is similar to the cutter almost never present. The other dredge pump rotates at 324 rpm or 5.4 Hz, with three blades the blade passing frequency is 16.2 Hz. The e-motors rotate at higher speeds of about 1000 rpm or 16.7 Hz. The diesel engine rotates at approximately the same speeds. The machine vibrations will be at a significantly higher frequency than the cutter or waves.

Table 4, Inventory of machinery and the nominal frequency

Source	Frequency
Dredge pump	16.2 Hz
Submerged Dredge pump	10.8 Hz
E- Motor	16.7 Hz
Diesel Motor	16.7 Hz

3.2.5 Combination

The wave frequencies are dominant in the lower regions of the spectrum, the cutter motions in the middle regions of the spectrum and the machinery in the upper parts of the spectrum. Space is remaining in the spectrum where there is room for vibration isolation. Namely $0.3\ Hz < f < 2Hz$ and $4Hz < f < 10Hz$.

Table 5, Inventory of the sources and their forcing frequencies

Excitation Source	Frequency Range
Waves	<0,3 Hz
Cutter head	2 - 3,5 Hz
Dredge pump	10 - 16 Hz
E-Motor	10 - 17 Hz
Diesel engine	10 - 25 Hz

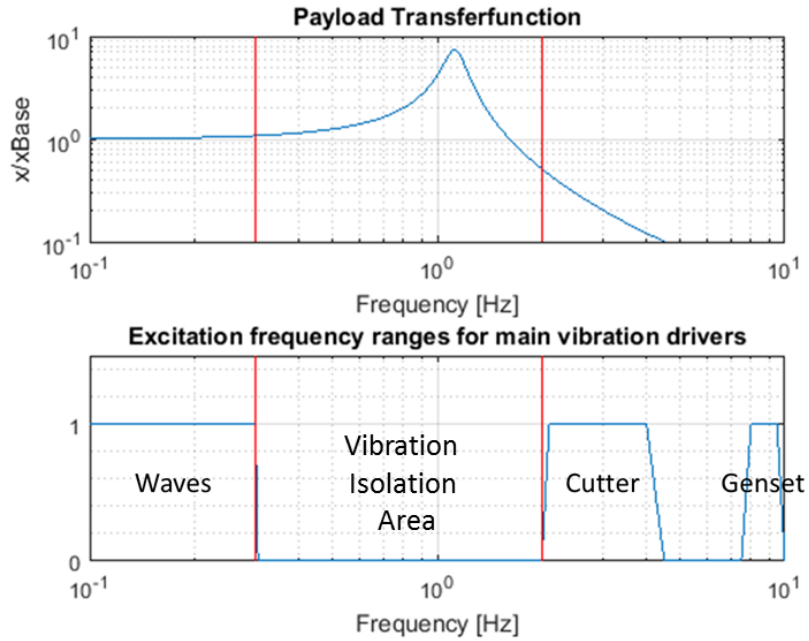

Figure 3-13, Overview of the vibration isolation area and excitation areas

3.3 Vibration isolation selection

Based on the theory in chapter 2 and the inventory in chapter 3, a promising type of vibration isolation will be selected in this section. Several options will be discussed along with their pros and cons. After that the most promising will be selected and further developed in chapter 4. The three types of vibration isolation that have been deemed the most interesting or promising are:

- Tuned mass damper
- Impact dampers
- Mechanical springs

A Tuned mass damper (TMD) is a large additional mass that is connected to the object to be isolated using springs. The motions of the additional mass are extracting energy from the object and thereby reducing its vibration amplitude. The downside to this system is that the additional mass has to be a minimum of 10% of the mass of the object (Lamancusa, 2002), making this an unnecessarily heavy solution. The second downside is that the isolation has to be achieved in more directions and the positioning of the secondary mass will greatly affect the motions in other directions.

Impact dampers are similar to a TMD however in this case the additional mass is not connected to the object to be isolated with springs but the impact of the mass is what transfers energy and thereby reduces the vibration amplitude. However the drawbacks of this system are: when the frequency of the vibrations is something that was not designed for the effectiveness is quickly lost and the mass required is again about 10% of the mass of the object (Zahrai, 2009).

Mechanical springs there are many kinds of mechanical springs like helical springs, rubber springs, leaf springs, wire rope springs and gas springs. The problem with many of these springs is that to get to a low enough eigenfrequency the static deformation becomes quite large(section 2.1.3). a number of these don't have load bearing capability for the mass that goes with the stiffness to produce the correct (linearized) eigenfrequency (Gopinah). Springs that are not loaded by gravity do not have these problems. Vertical isolation in the form of Rubber springs, helical springs or wire rope isolators could not be obtained with these characteristics. There were two mechanisms that had the potential to be used as a low eigenfrequency isolator: a gas spring and a negative stiffness mechanism (Platus, 1993). The use of gas springs was deemed too expensive by the client and therefore this thesis continues with negative stiffness mechanisms as the vibration isolation of choice. The cabin will be only vertically isolated with NSMs the horizontal directions are solved with helical low stiffness springs.

3.4 Conclusion

Cause of the current vibration issues is resonance. The resonance is caused by the overlap between the third natural frequency and the operational frequency of the cutter. The isolation of vibrations at the source is not practical due to the fact that there are multiple sources at different locations. Application of isolation at the base of the cabin appears to be feasible. The other vibration sources are the engines and the waves. These two sources are present In other vessels for example those used for shipping. These vibrations can be isolated using rubber isolators. Cutter vibrations have to be isolated using another type of isolation. This isolation can be designed to have an eigenfrequency in between the forcing frequency of the waves and the cutter.

The current setup with a cabin on springs combined with the intervals between the wave excitations and the cutter excitations can be adapted to suit the properties of low frequency vibration isolation. The precise isolators will be evaluated in the theoretical dynamics section of the report.

Standard low stiffness springs are not feasible for this type of isolation due to the large static deflection. The most promising solutions are negative stiffness mechanisms and gas springs. Between these two solutions, low frequency vibration isolation in the form of a Negative Stiffness Mechanism was deemed the most promising and the research will continue with these in chapter 4.

4 Theoretical modelling

In chapter 3 the decision was taken to approach the vibration issues with the use of a negative stiffness mechanism (NSM). In this section, the theoretical background of the negative stiffness mechanism and its behaviour will be determined. There are several different practical solutions for the NSM however all are based on the same principle. The principles of an NSM will be discussed in section 4.1. In section 4.2 the workings and modelling of an NSM is discussed. In section 4.3 the use of the NSM in a six degrees of freedom (6DoF) system will modelled and explained.

4.1 Negative stiffness mechanism

The reasons for the choice of the NSM are summarised below:

- Large deformations under gravity load and due to additional loading
- No industrial spring available for the low stiffness while possessing load bearing capacities
- High costs associated with gas-springs.
- Conventional springs cannot obtain low enough stiffness properties due to the material properties of the springs.

A Negative stiffness mechanism is in essence an instability mechanism. The instability leads to tendency to try and buckle outwards when small forces are applied. This buckling gives then an extra force in the direction of the original load. This extra force works opposing a positive spring force introduced by a conventional spring. The extra force opposes the load exerted by the main spring and is thereby reducing the stiffness of the complete system. The reduction of the stiffness is what gives the NSM its name.

The positive-negative stiffness mechanism essentially looks like Figure 4-1 .

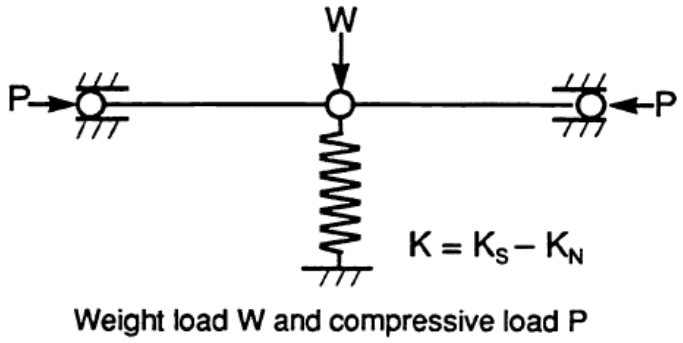

Figure 4-1, Negative-positive stiffness mechanism

There are several options with which the effects of Negative stiffness can be achieved. The main spring component does not change in essence. The options for the NSM are:

- The post-critical buckling element
- The bending element with or without hinge
- The rigid bar with hinges

The post critical buckling element has the preload $[P]$ lower than the critical buckling load. The preload is affected by the geometry and the material properties of the buckling element. Once the geometry is set the NSM properties can only be changed with changes to or replacement of the buckling elements. The properties of this system can be tweaked by choosing the appropriate bar length, the area moment of inertia of the profile and the material type.

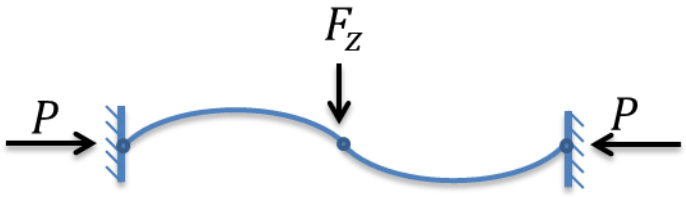

Figure 4-2, Post-critical buckling element with hinges

The bending element is a positive spring of itself however when the preload is large enough is becomes a NSM. Tweaking this system to have the correct properties can be done by choosing the bar length, area moment of inertia of the profile and material type. The changing of the properties of the system is achieved by switching out the bars.

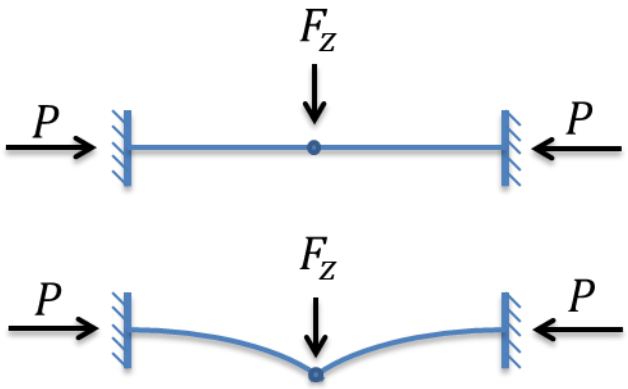

Figure 4-3, Bending element with hinge

The rigid bar element is made up of three hinges with two rigid bars in between. The bars have to be heavy and strong enough to withstand the preload. The mechanism can be tweaked with the bar length and the preload $[P]$. The way the preload is applied can also be varied to obtain the required system properties.

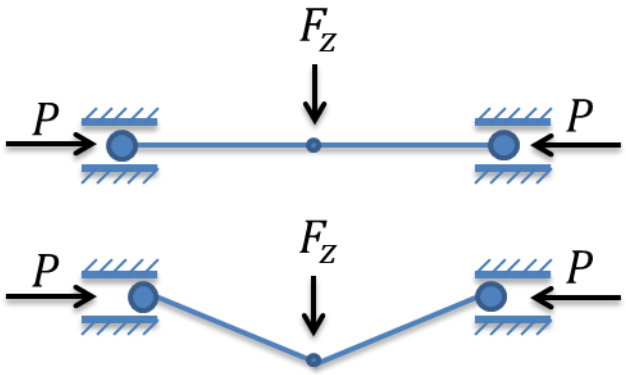

Figure 4-4, Rigid bar element

The preferred type of NSM is the rigid bar, in the system shown in Figure 4-1 the capacity to resist vertical loads is of interest. The assumption is made that the positive z direction is upwards and a positive force is exerted by the vertical (main) spring. The total load exerted by the positive-negative stiffness mechanism is:

$$F\text{-}_{total} = F_{z.Spring} + F_{z.NSM} \tag{58}$$

The different contributions will be further discussed in this section.

4.1.1 Stiffness of the mechanism

The vertical force exerted by the main spring or primary spring is assumed to be linear. The forcing $[F]$ is:

$$F_{z.Spring} = k_1 \cdot z \tag{59}$$

The derivative $\left[\frac{df}{dz}\right]$ of this function is called the stiffness $[k_1]$.

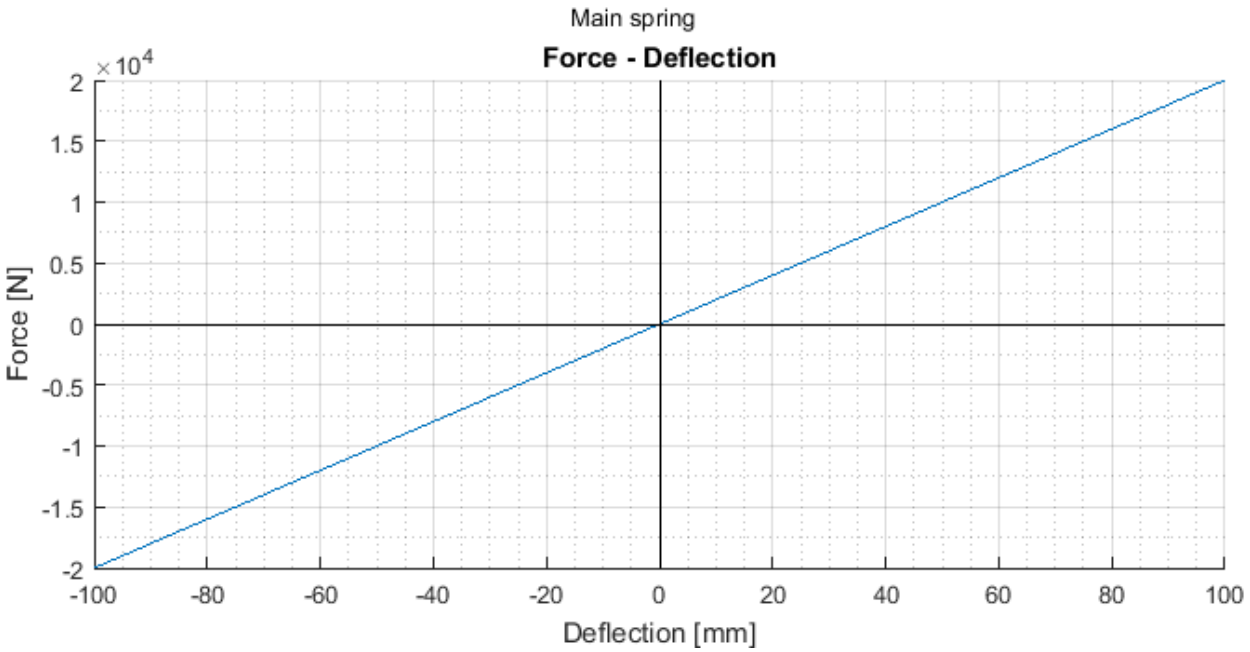

Figure 4-5, Force deflection diagram for main spring

The system described in this section is the system shown in Figure 4-4. This system can be configured in multiple ways. The negative stiffness force for this setup can be found as a function of the preload [P], the length of the arms [L] and the deflection [z]

$$F_{z.NSM} = -2 \cdot P \cdot \tan\left(\arcsin\left(\frac{z}{L}\right)\right) \tag{60}$$

This can also be written as:

$$F_{z.NSM} = -2 \cdot P \cdot \frac{\frac{z}{L}}{\sqrt{1-\frac{z^2}{L^2}}} \tag{61}$$

The stiffness $[k_{NSM}]$ is what is really interesting for the reduced stiffness and is given by:

$$k_{NSM} = \frac{dF_{NSM}}{dz} = \frac{d}{dz}\left(-2 \cdot P \cdot \frac{\frac{z}{L}}{\sqrt{1-\frac{z^2}{L^2}}}\right) = \frac{-2 \cdot P \cdot L}{(L^2 - z^2) \cdot \sqrt{1-\left(\frac{z}{L}\right)^2}} \tag{62}$$

For small $(z \approx 0)$ values of the deflection $[z]$ the stiffness can be expressed in a simplified form and the preload can be easily calculated with respect to the mainspring stiffness.

$$k_{NSM}(z \approx 0) = -2 \cdot \frac{P}{L} + O(z^2) \tag{63}$$

If the preload [P] is assumed as a constant force, the load – deflection graphs of the NSM are shown in Figure 4-7.

$$F_{Total} = k_1 \cdot z - 2 \cdot \frac{P}{L} \cdot z, \qquad z = 0 \tag{64}$$

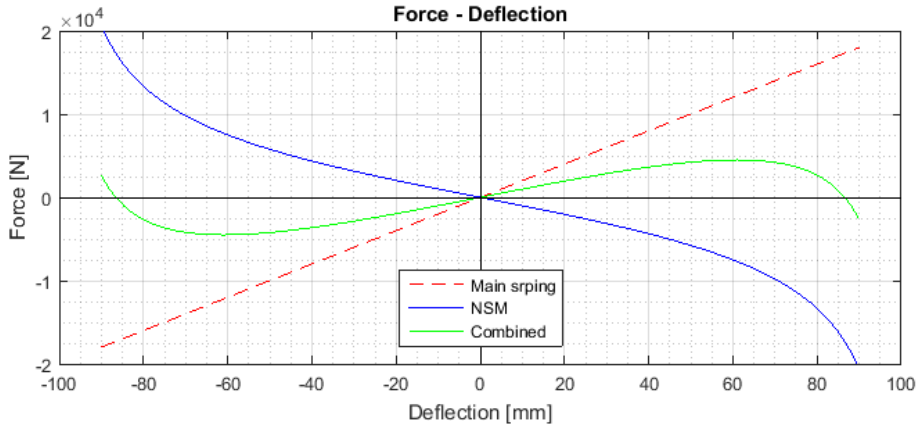

Figure 4-6, Force- deflection graph for NSM with constant preloading force

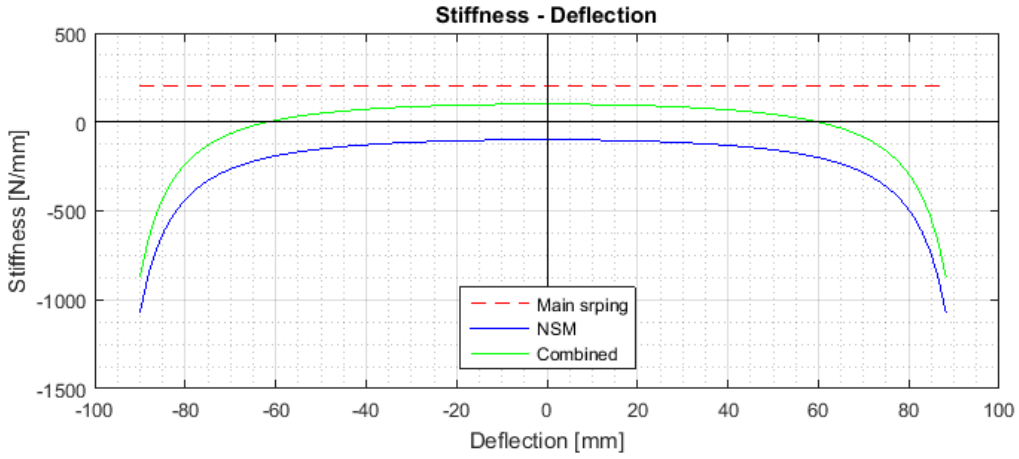

Figure 4-7, stiffness- deflection graph for NSM with constant preloading force

4.1.2 Spring preloaded negative stiffness mechanism

A constant load could probably be achieved but it might be just as easy to use a spring for the preload [P]. in Figure 4-8 the negative stiffness part of the spring preloaded mechanism is shown. In which $[L_s]$ is the length over which the secondary spring $[k_2]$ is compressed in order to get the proper preload value, $[\Delta L]$ is the length change in the secondary spring due to the deformation of the system.

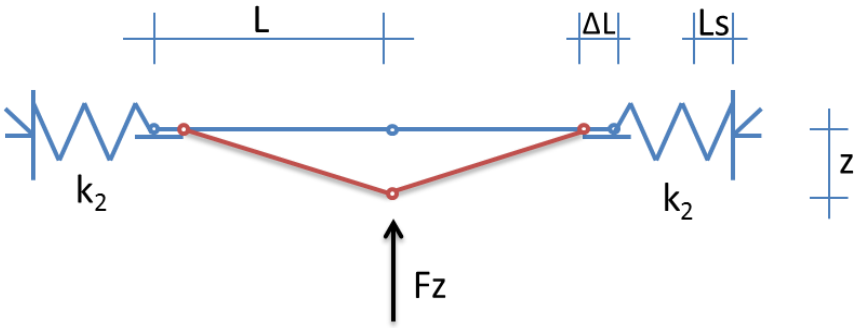

Figure 4-8, Negative stiffness mechanism spring preloaded

The most important difference with respect to the system with a constant preload [P] is that the preload becomes dependent on the deflection.

$$P = k_2(L_s - \Delta L) \tag{65}$$

$$\Delta L = L \cdot \left(1 - \cos\left(\arcsin\left(\frac{Z}{L}\right)\right)\right) \tag{66}$$

Can be written as:

$$\Delta L = L \cdot \left(1 - \sqrt{1 - \frac{z^2}{L^2}}\right) \tag{67}$$

The entire negative stiffness equation now becomes:

$$F_{z.NSM} = -2 \cdot k_2 \left(L_s - L * \left(1 - \sqrt{1 - \frac{z^2}{L^2}}\right)\right) \cdot \frac{\frac{z}{L}}{\sqrt{1 - \frac{z^2}{L^2}}} \tag{68}$$

The graphs for this are shown in Figure 4-9.

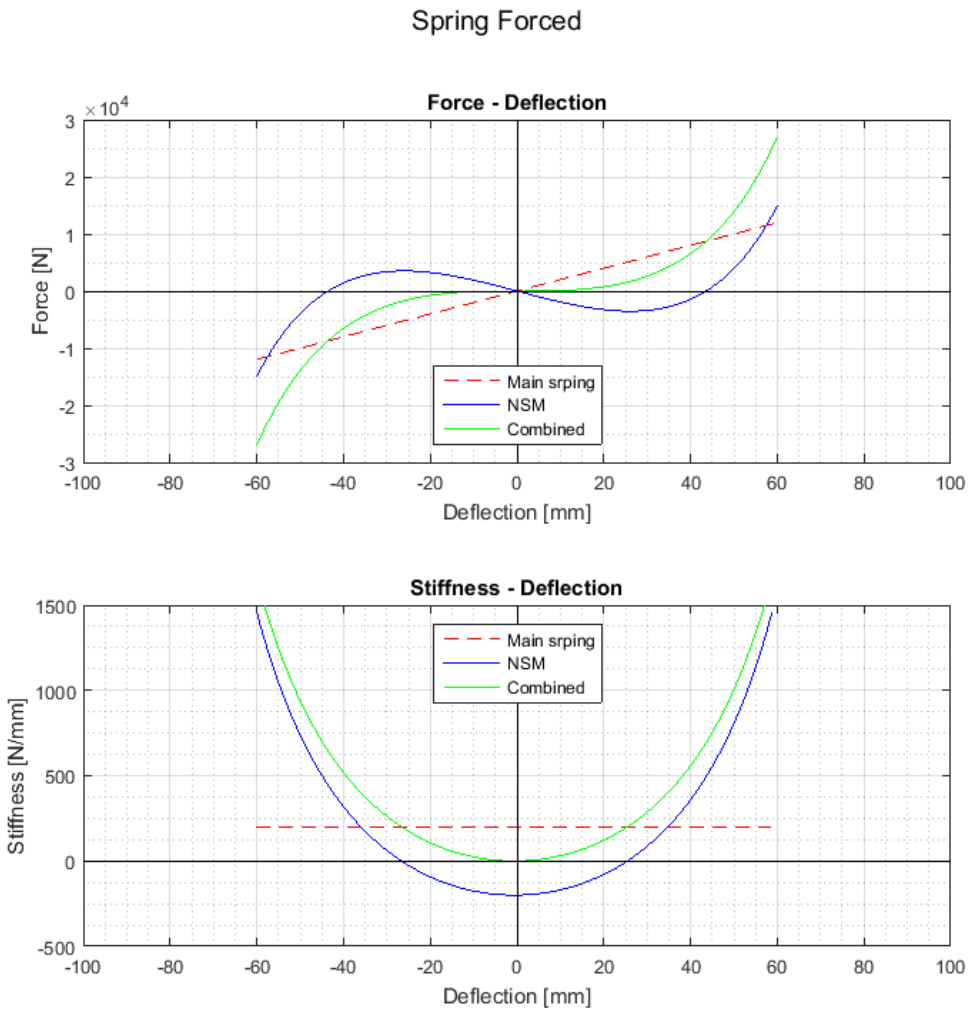

Figure 4-9, F-z and dF/dz –z graphs for NSM with spring preloading

Different parameter choices for the NSM result in different shapes on the Forcing and the Stiffness curves.

4.1.3 Designing an NSM

Design of a proper NSM for a system is based on the amount of parameters that can be changed. The amount of parameters appears to be very large however due to the dependence on each other the amount of parameters that can be changed is limited.

$$F_z = k_1 \cdot z - 2 \cdot k_2 \left(L_s - L \cdot \left(1 - \sqrt{1 - \frac{z^2}{L^2}} \right) \right) \cdot \frac{\frac{z}{L}}{\sqrt{1 - \frac{z^2}{L^2}}} \tag{69}$$

$$k_z = k_1 - 2 \cdot \frac{k_2 \left(L_s \cdot L + L^2 \left(\sqrt{1 - \frac{z^2}{L^2}} - 1 \right) - z^2 \sqrt{1 - \frac{z^2}{L^2}} \right)}{(L^2 - z^2) \cdot \sqrt{1 - \frac{z^2}{L^2}}} \tag{70}$$

$$k_z = \frac{dF_z}{dz} = k_1 + \frac{k_2 \left(-2 \cdot L \cdot L_s + 2 \cdot z^2 \cdot \sqrt{\left(1 - \frac{z^2}{L^2} \right)} + L^2 \left(2 - 2 \sqrt{\left(1 - \frac{z^2}{L^2} \right)} \right) \right)}{(L^2 - z^2) \cdot \sqrt{\left(1 - \frac{z^2}{L^2} \right)}} \tag{71}$$

When the NSM is setup properly the deflection without any forcing is set to zero $[z = 0]$. When the deflection equals zero the stiffness constraints still apply, resulting in a system of simplified equations which will be used for the preliminary design guide of an NSM.

$$k_z(z = 0) = k_1 - 2 \frac{L \cdot k_2 \cdot L_s}{L^2} = k_1 - 2 \cdot \frac{P}{L} \tag{72}$$

The design of an NSM is based on the isolation frequency $[\omega_{is}]$. Since the mass of the object to be isolated is often determined by other factors than the isolation and the eigenfrequency is determined by the forcing frequencies, the required stiffness $[k_z]$ can be derived using the mass and the eigenfrequency.

$$\omega_{is} = \sqrt{\frac{k_{req}}{m}} \rightarrow k_{req} = \omega_{is}^2 \cdot m \tag{73}$$

The variables that can be changed to obtain an optimal NSM are: bar length $[L]$, main spring stiffness $[k_s]$, NSM stiffness $[k_{NSM}]$, preload $[P]$, secondary spring stiffness $[k_2]$ and preload length $[L_s]$.

The properties of the NSM are tied into the required stiffness and the available springs. The main spring stiffness is chosen based on the allowable gravitational deflection $[\delta]$ (see section 2.1.3 for more information). If the gravitational deflection is no restricting issue the lowest stiffness available while still

capable of bearing the load will be selected. Having k_s and k_z known the stiffness that the NSM has to provide is also known

$$k_z = k_1 + k_{NSM} \tag{74}$$

The required stiffness is a function of the preload and the bar length. The effects of different preload with the same bar length can be seen in Figure 4-12 due to the change in preload a change in stiffness occurs. The change is consistent with the theory presented in section 4.1.2.

$$k_{NSM} = -2 \cdot \frac{P}{L} \tag{75}$$

Since the stiffness is known the preload and the length are dependent on each other and only one truly independent variable remains. The bar length can be changed arbitrarily. However for longer bar lengths the preload increases . The length of the bar affects several other design parameters as well. The linear behaviour of the system is influenced through the angle parameter $\left[\frac{z}{L}\right]$. When a larger bar length is selected, the deflection for which the system responds in a linear manner is increased. In Figure 4-10 these effects are shown.

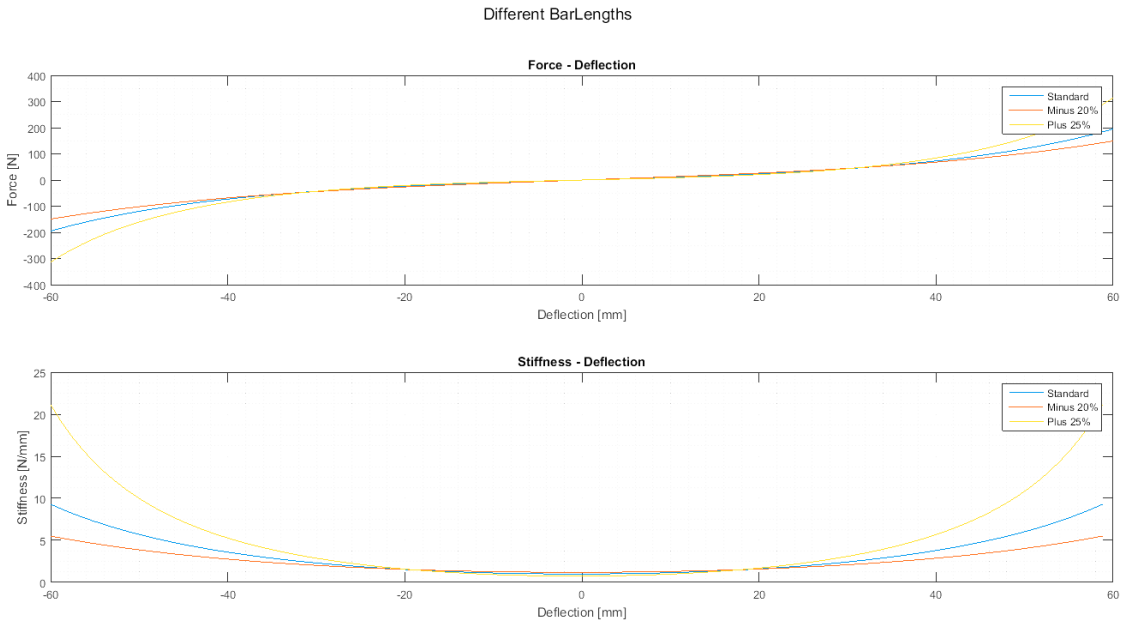

Figure 4-10, Differen Barlengths

When a spring loaded NSM is used the preload is equal to the secondary stiffness times the preload length. In Figure 4-11 the effects of changes in the secondary spring coefficient are shown. When the secondary spring is chosen to be stiffer, the non-linearity of the stiffness curve increases.

$$P = k_2 * L_s \tag{76}$$

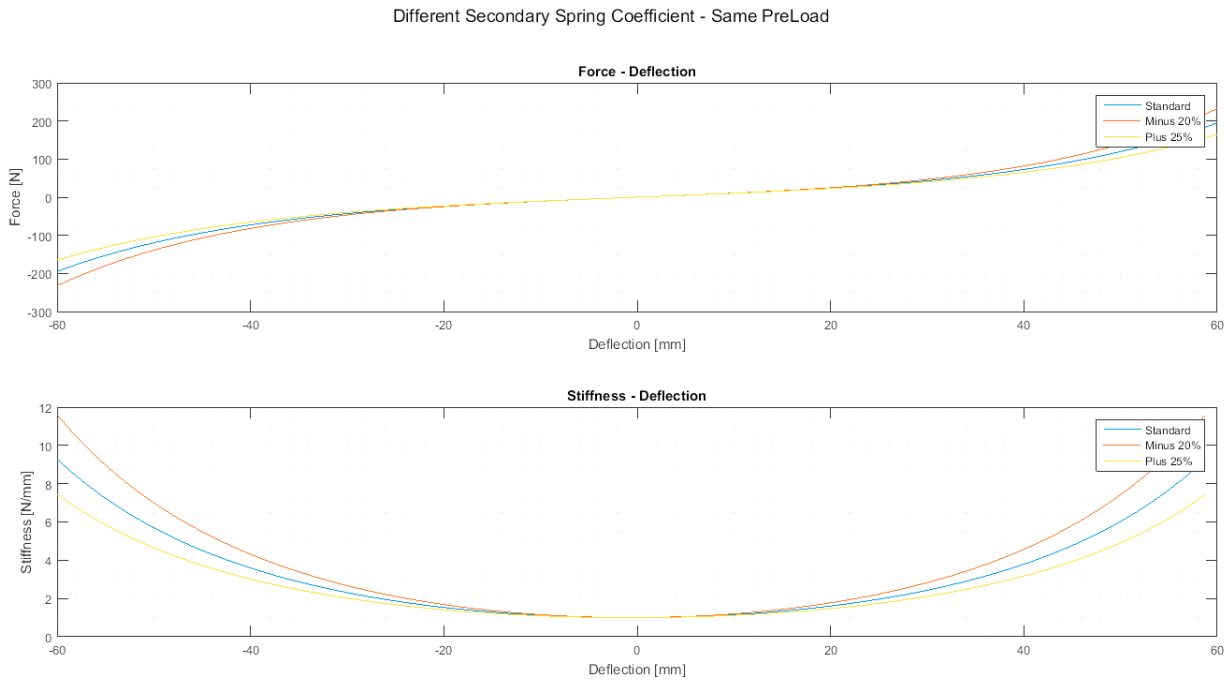

Figure 4-11, Different secondary spring coefficient - same preload

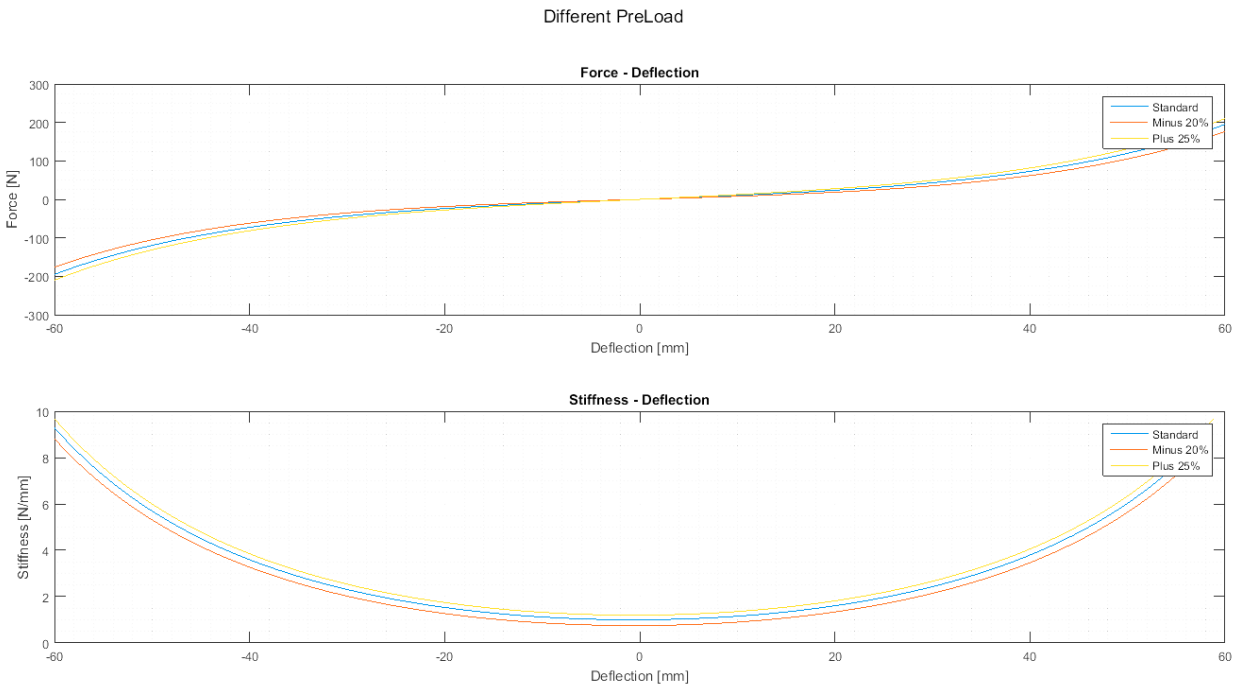

Figure 4-12, Different preload

4.1.4 Conclusions

- The main spring stiffness is dependent on its load bearing capabilities, preferably the stiffness is the minimum stiffness available while maintaining the loadbearing capabilities.
- The required negative stiffness is dependent on the isolation frequency $[\omega_{is}]$ of the vessel-OC system and the main spring stiffness. The required negative stiffness is reached by a combination of bar length and pre load.
- The bar length is dependent on the amount of stroke required for the system, which results in a minimum length and the possibility to reduce the required preload by the inverse length therefore the bar length should be the minimum required for the stroke.
- The preload is the loading applied in horizontal direction. The magnitude of this load Is determined by the required negative stiffness and the bar length.
- The stiffness of the secondary spring is determined by the stroke length, the stiffness should be sufficient to reverse the loading direction reverses before the maximum stroke is reached.
- The preload length of the spring is determined by the stiffness of the secondary spring and the required stiffness

4.2 Negative Stiffness Model

The modelling of the negative stiffness mechanism is discussed hereafter. To prove the effects of the NSM on the stiffness of the overall system, the NSM is modelled. The overall setup will be discussed in section 4.2.1.

The geometry of the model is shown in Figure 4-13. The modal shapes in Figure 4-14. Further down the line the force and base transfer functions are shown, linearized around the static equilibrium. After the transfer functions a time simulation is shown. The time simulation is analysed by switching to the frequency domain and observing the data.

4.2.1 Model setup

The model is set up with bodies and forces, the bodies are: the payload, two links horizontal, two Links vertical and the base. The vertical links are connected at their bottom to the base with hinges that allow rotation around the local x axis and no displacement. The top is similarly connected to the horizontal links except these hinges can displace. The horizontal hinges are connected to the payload with the same hinges. The point of connection to the payload is outside of the payload itself for modelling purposes.

The other items are the secondary springs and the main spring. The secondary springs are connected at one side to the base with a rigid connection that in not shown in Figure 4-13. The other end is connected to the end of the Horizontal Links. The main spring is connected to the Base at the bottom and the centre of gravity (CoG) of the payload.

The main spring is setup to provide the damping in the further undamped system. The damping is set up as a modal damping of 3%. The modal damping is dependent on the eigenfrequency of the complete system but applied to the main spring.

The EoM for a linear damper and a stiffening spring can be approximated by using a geometrical non-linearity. Resulting in a stiffness that is only dependent on the displacement $[x]$. The EoM for a base excitation is written as:

$$m\ddot{x} = F_k + F_c + F_{external} \tag{77}$$

In which the damping and the stiffness forces can be changed for:

$$m\ddot{z} = c \cdot (\dot{z}_b - \dot{z}) + F_k(z, z_b) \tag{78}$$

In which

$$c = 0.03 \cdot 2 \cdot \sqrt{m \cdot k(0)} \tag{79}$$

$$F_k = k_1 \cdot (z - z_b) - 2 \cdot k_2 \left(L_s - L * \left(1 - \sqrt{1 - \frac{(z-z_b)^2}{L^2}} \right) \right) \cdot \frac{\frac{(z-z_b)}{L}}{\sqrt{1 - \frac{(z-z_b)^2}{L^2}}} \tag{80}$$

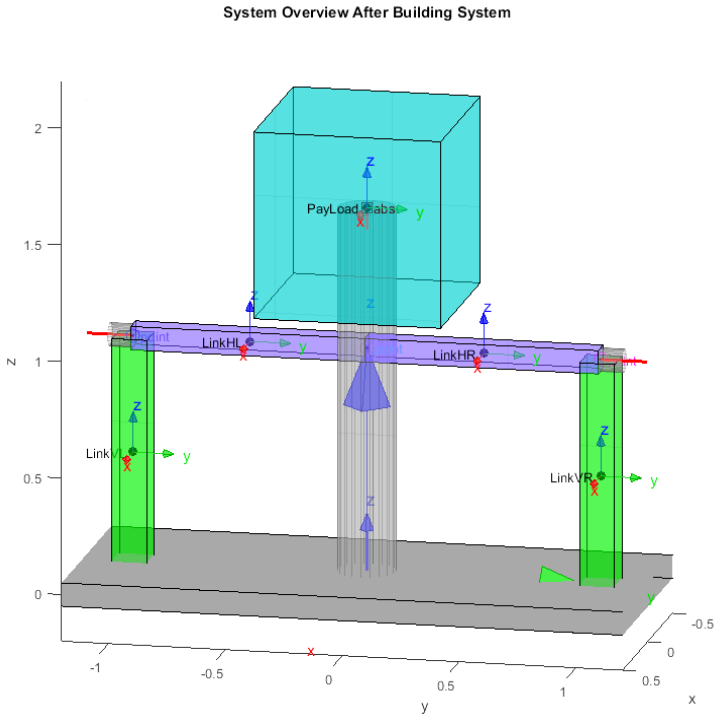

Figure 4-13, Model overview

4.2.2 Linearized solutions

The system is nonlinear however, for small amplitude vibrations (base amplitudes < 5mm) the system behaves linearly. The solutions obtained for the linearized system are valuable especially outside the amplification range of the system, as the system should behave linearly in those regions and then the hand calculations will suffice for engineering purposes.

In the model, the system is first linearized around the equilibrium point then the eigenfrequencies and eigenvectors are calculated. In Figure 4-14, the eigenvector for the eigenmode (z motion) is plotted in the positive and negative direction, resulting in the linearized modal shape.

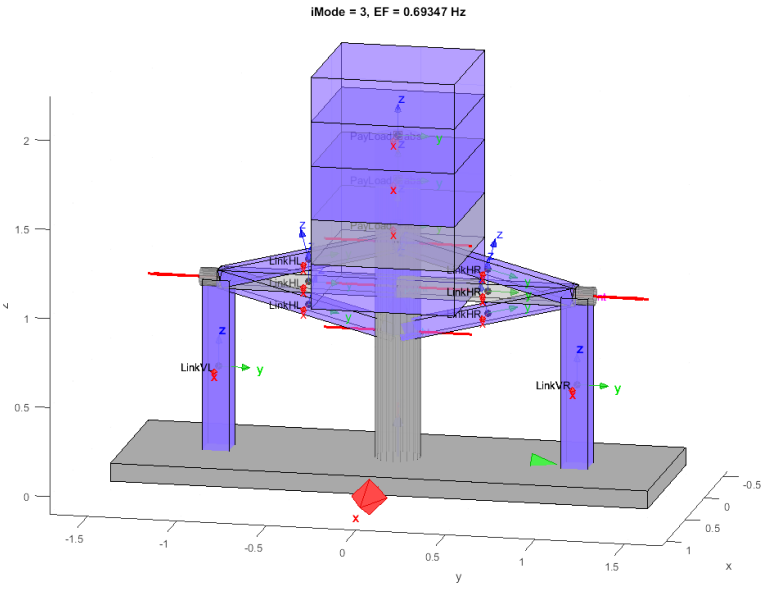

Figure 4-14, Modal Shape

The Base-payload transfer function seen in Figure 4-15 is based on the linearized eigenfrequency and the damping of the system. In the figure the lines indicate the end and start of the forcing frequencies. In between the lines there will be no excitation. The resulting reduction of the vibration amplitude at 2Hz will be 50% and for the 4Hz vibrations the reduction will be 85%.

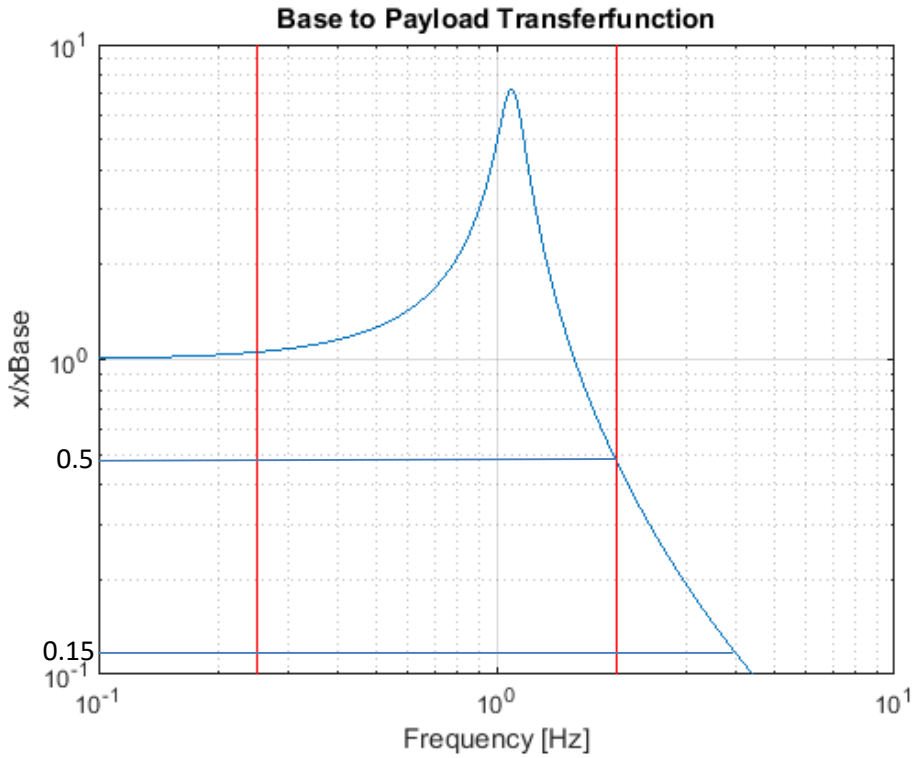

Figure 4-15, Base - payload transfer function

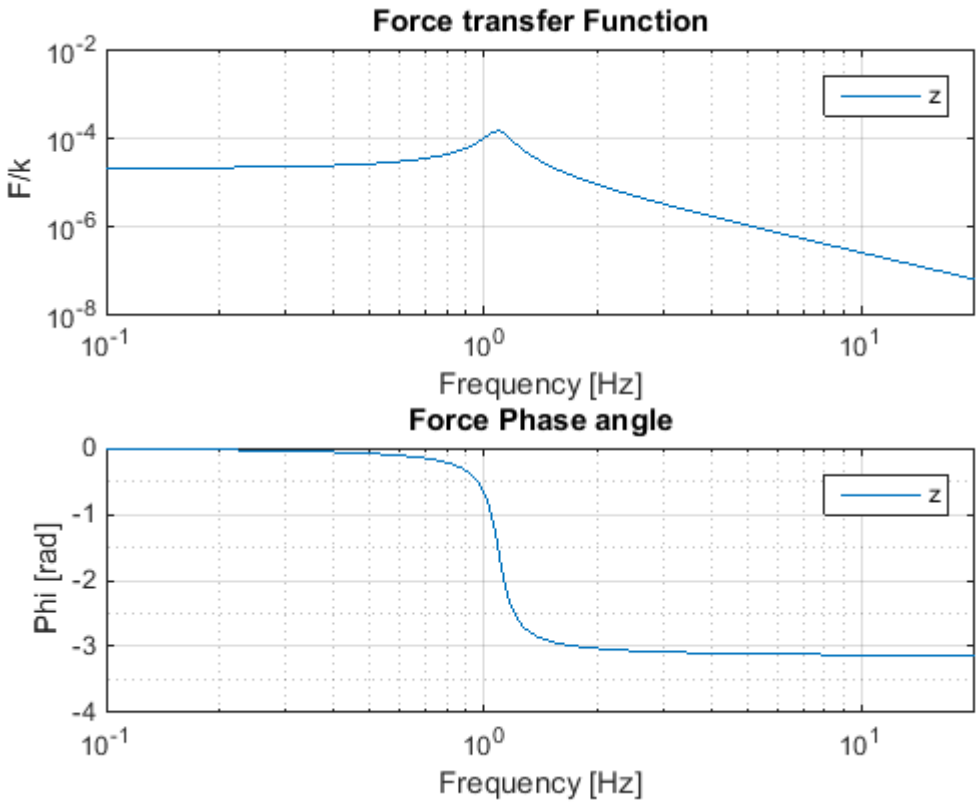

Figure 4-16, Direct loading of payload Bode Plot

4.2.3 Nonlinearity

The mechanism show in Figure 4-13 has a different stiffness for different displacement values. The actual force - displacement graph is shown in Figure 4-17 alongside the stiffness – displacement graph. The figure shows that the stiffness is lower around the equilibrium point but higher farther away. The stiffening behaviour as mentioned in section 2.1.

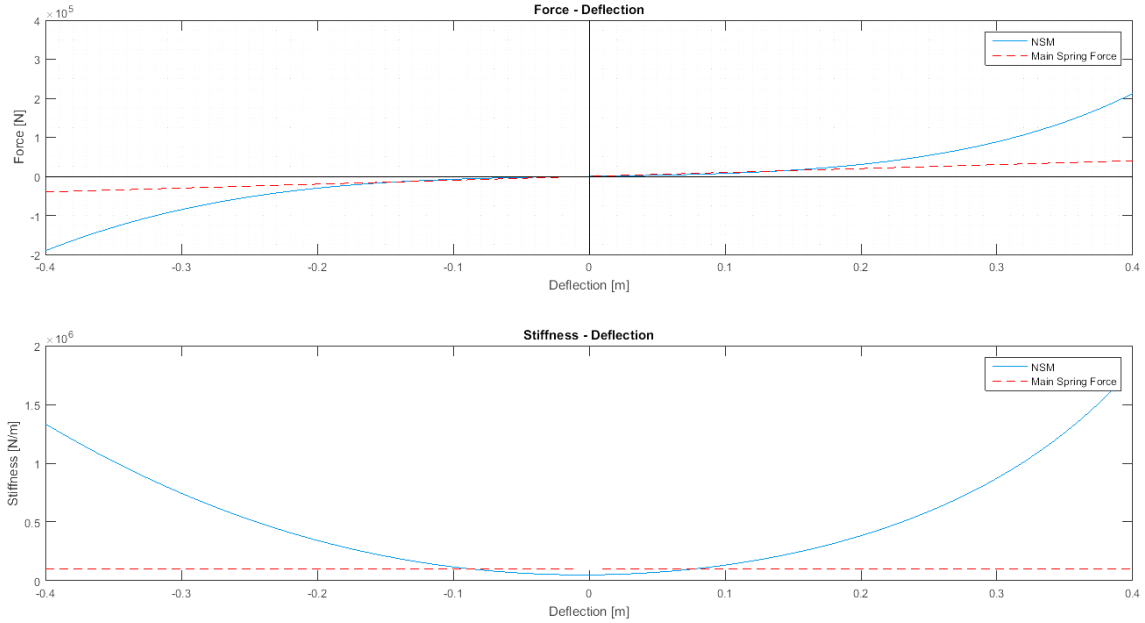

Figure 4-17, Force-displacement graph

4.2.3.1 *Nonlinear transfer function*

The true behaviour of the system is non-linearly dependent on the amplitude and frequency of the excitation. Therefore the linearized system of equations is exchanged for time simulation for different frequencies and different amplitudes. The nonlinear transfer functions are obtained by sampling the maxima of the spectra after some time to allow the damp out of the transient motion.

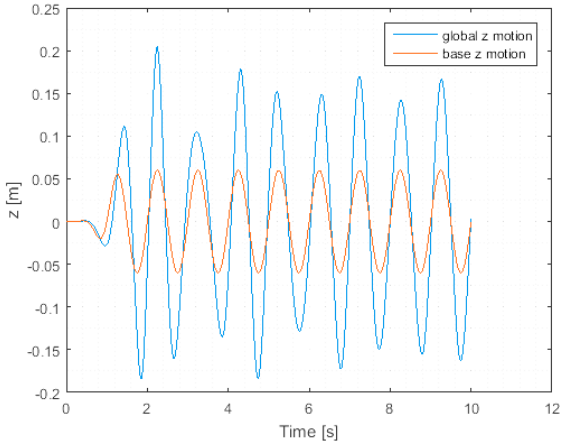

Figure 4-18, Time series example

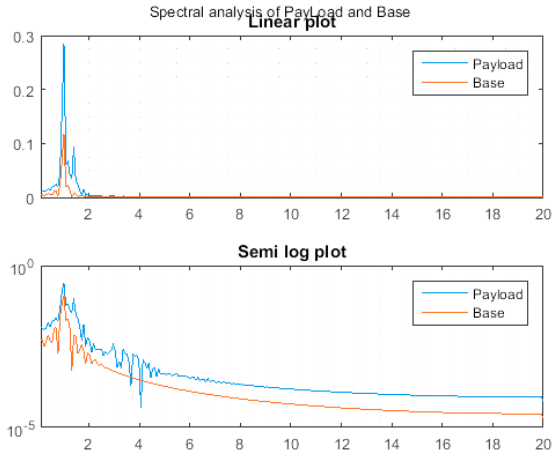

Figure 4-19, Spectrum from Time Series example

The resulting graph is shown in Figure 4-20 in which the maxima of the steady state solution are plotted versus the excitation frequency. In Figure 4-21 the results are normalised with respect to the excitation amplitude. In the figures there are some numerical oddities visible. These oddities are based on the way the maximum is determined from the time series to achieve the transfer function. If the amount of samples is too small, the second order wave motions are introduced in the plots. A more accurate representation would be achieved when the sampling time is increased. The sampling time increases the time required for the simulation. The increased sampling method is applied to get the results shown in Figure 4-20 and Figure 4-21.

4.2.3.2 Second order Wave motions

When the eigenfrequency of the equivalent linear system and the forcing frequency approach each other, the difference between the eigenfrequency $[\omega_n]$ of the equivalent linearised system and the forcing frequency $[\omega]$i.e. $[|\omega_n - \omega|]$ starts to play a significant role. This frequency behaviour causes an envelope around the forcing frequency response function. This envelope reduces and amplifies the frequency response this is called the beating phenomenon.

4.2.3.3 Results

In Figure 4-20 and Figure 4-21 the results of the 1DoF modelling are shown. The main result is the transmissibility for different base amplitudes. The amount of non-linearity in the system increases, this is indicated by steepening of the right side of the peak. The non-linearity has the effect that the dynamic amplification factor is lowered and that the eigenfrequency shifts to the higher region, consistent with a higher stiffness.

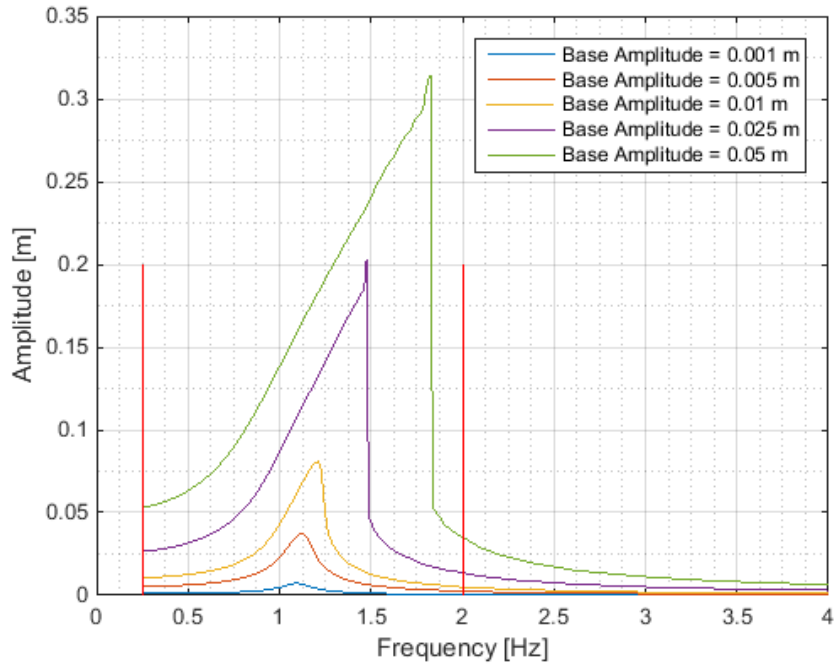

Figure 4-20, Transmissibility (base-payload)

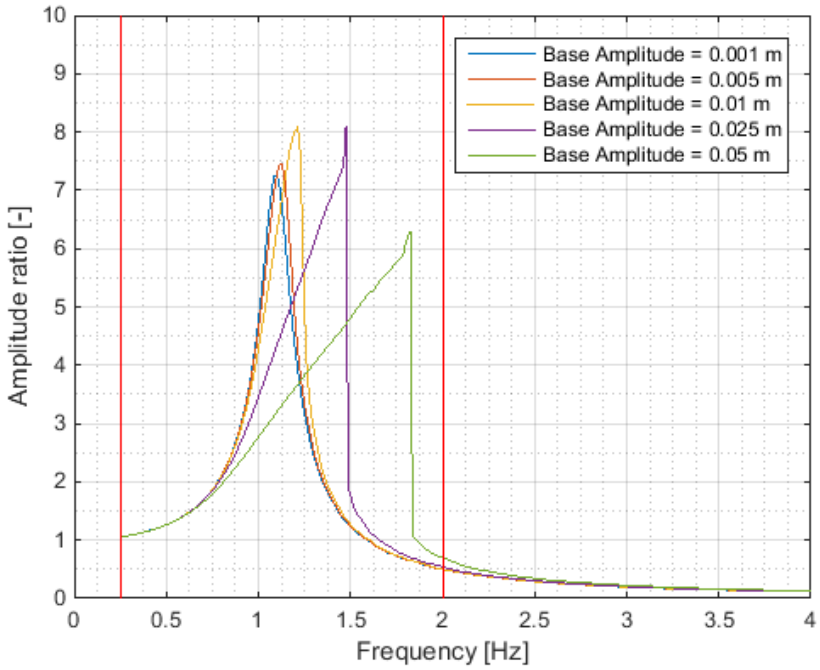

Figure 4-21, Transmissibility (base-payload) normalised

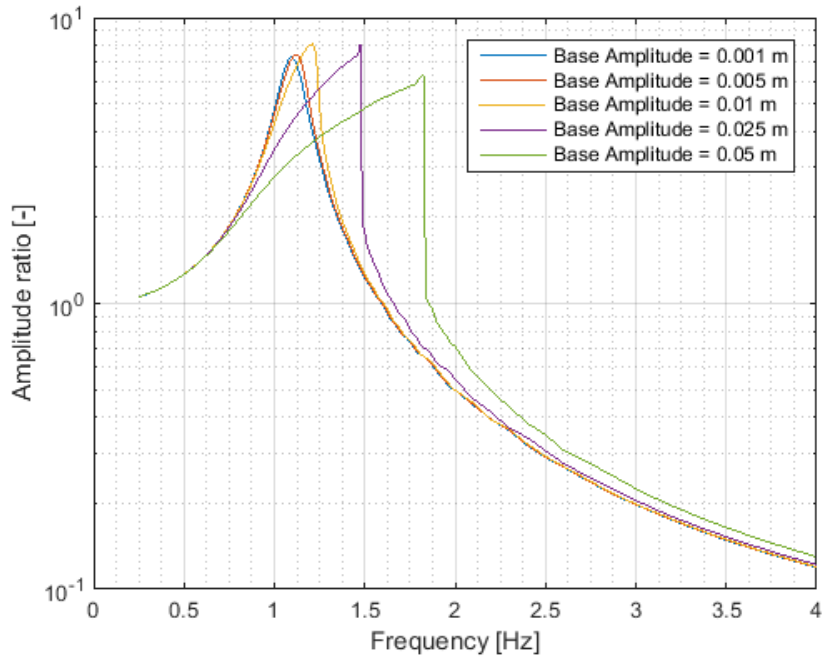

Figure 4-22, Transmissibility (base-payload) normalised semi-log

4.2.4 Conclusions

The effects of the non-linearity become more pronounced for the higher amplitude of the base excitation. When this happens the peak frequency shifts increases. The shift of the eigenfrequency brings it closer to the undesired region. This effect is detrimental to the functioning of the system. Attempts to lower the initial eigenfrequency do not have a positive effect since the lower amplitude vibrations the system could then come into the lower undesired region. This effect can be countered by choosing the appropriate bar length for the system based on the $\left[\frac{z}{L}\right]$ ratio. The model further indicates that the system can function properly outside the vibration isolation rang applies for the single degree of freedom system. The non-linearity of the system causes the vibration amplification region to expand reducing the vibration isolation area and the effectiveness of the vibration isolation. Non linearity due to stiffening of NSM causes lower amplification factor than linear system. this means that even if there is resonance, the amplitudes are limited to about half of what a linear system with the same damping would experience in resonance.

4.3 Six degrees of freedom model

The behaviour of the OC cannot be described by a single degree of freedom. The OC, when considered as a rigid block, has six degrees of freedom. The goal of this section is to prove that the NSM solution is feasible for the use on CSDs. Section 4.2 described the principle behaviour of the NSM in a one dimensional setting. The complete picture can only be obtained when implementing the NSM in a three dimensional setting. Therefore the complete system is modelled by separating the springs into three directions at four points (the NSM is activated only in the heave direction). The vertical springs have the characteristic of the NSM obtained by the one degree of freedom model.

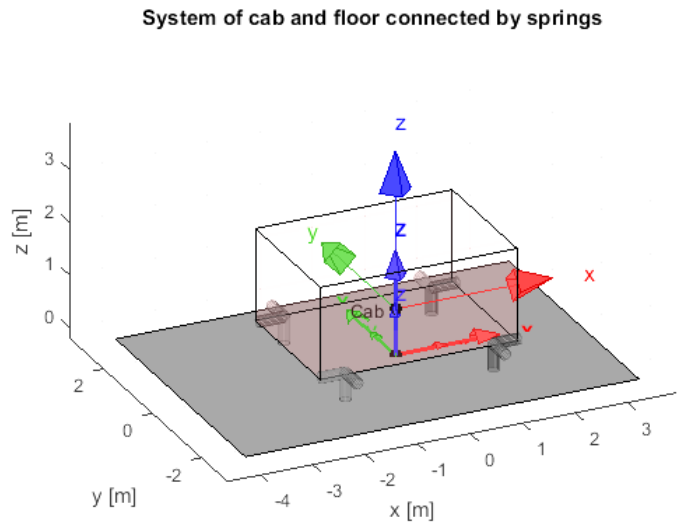

Figure 4-23, Model overview

The locations of the springs affect the eigenfrequencies of the system for the roll, pitch and yaw motions as well as the coupling terms of the system. The coupling terms determine the influence one motion has on another motion.

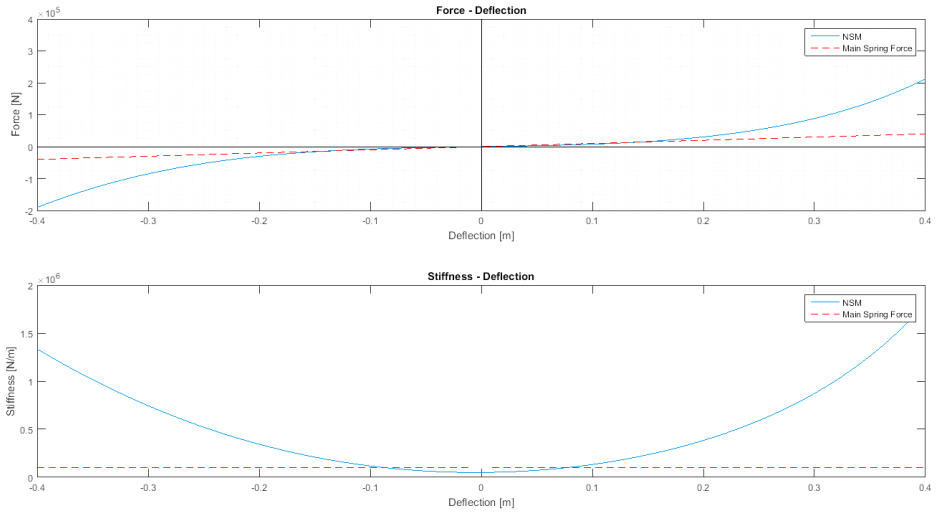

Figure 4-24, Force-displacement graph for singe vertical spring

4.3.1 Mode shapes

A linear system with six degrees of freedom has six eigenfrequencies and six eigenmodes belonging to the frequencies. The system is setup in such a way that the eigenfrequencies are closely located around 1 Hz which is the target isolation frequency. The frequencies and the mode shapes are shown in Figure 4-25. The mode shapes are a representation of the motions which the system will behave in when the system is excited with the corresponding frequency. These frequencies can be affected by the properties of the springs and their positioning. The rotational DoFs are affected by the position and the stiffness of the springs, when the springs are positioned further from the CoG the frequency of the rotation DoFs increases, that is the same with stiffening of the springs. The translation DoFs are only affected by the stiffness of the springs. This is similar to an SDoF system.

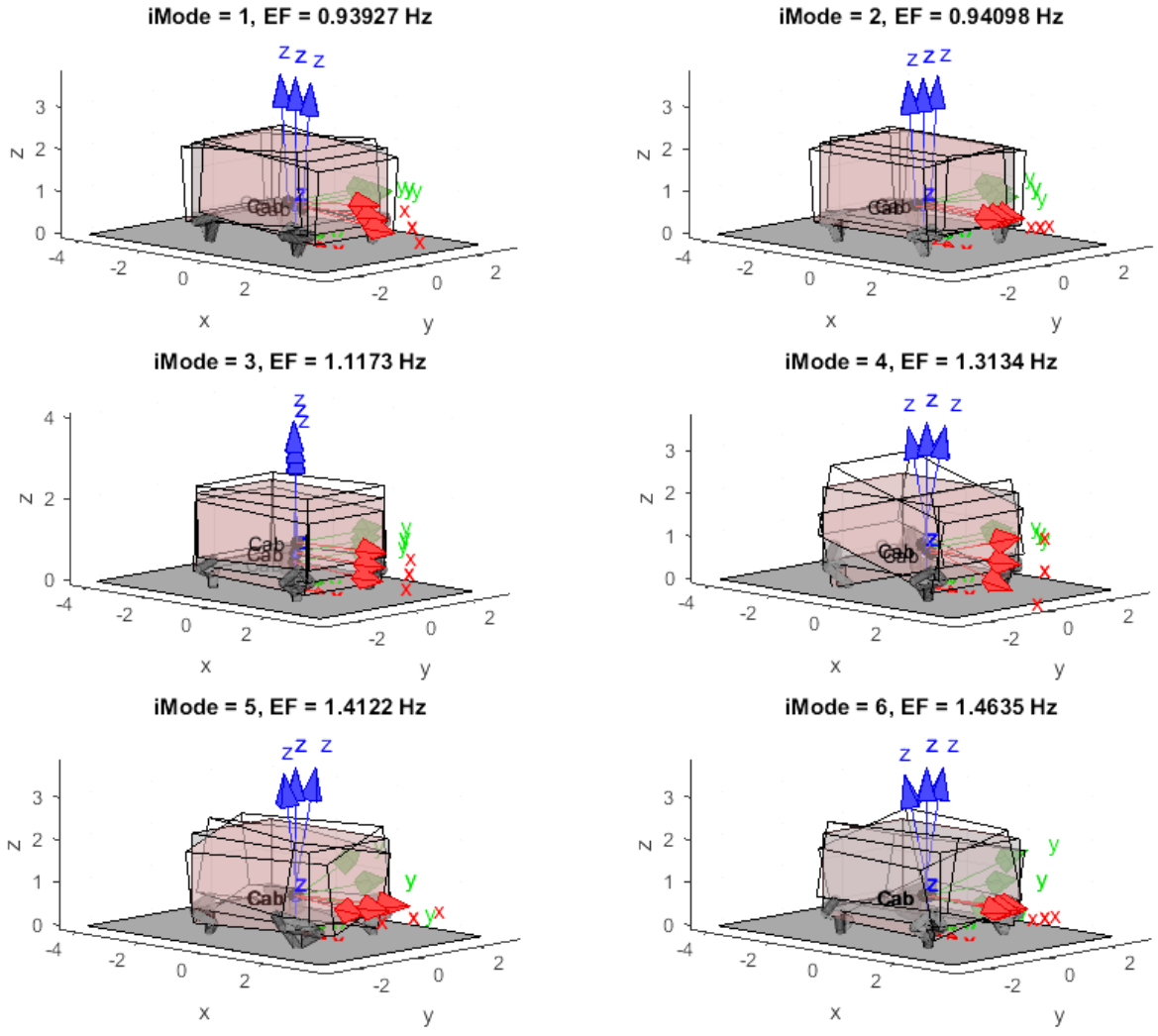

Figure 4-25, Eigenmodes of the system

4.3.2 Transfer functions

The linearized transfer functions around the equilibrium position show the system behaviour for small excitations. Larger excitations are influenced by the non-linearity of the system. The response to these larger amplitudes will have to be numerically modelled by time simulations as the response will generally depand strongly on the excitation amplitude (see Figure 4-20). The diagonal transfer functions of the main directions are shown in Figure 4-26, all transfer functions are shown in Figure 4-27. In Table 6 the directions are explained the transfer functions are set up as a transfer between base and payload.

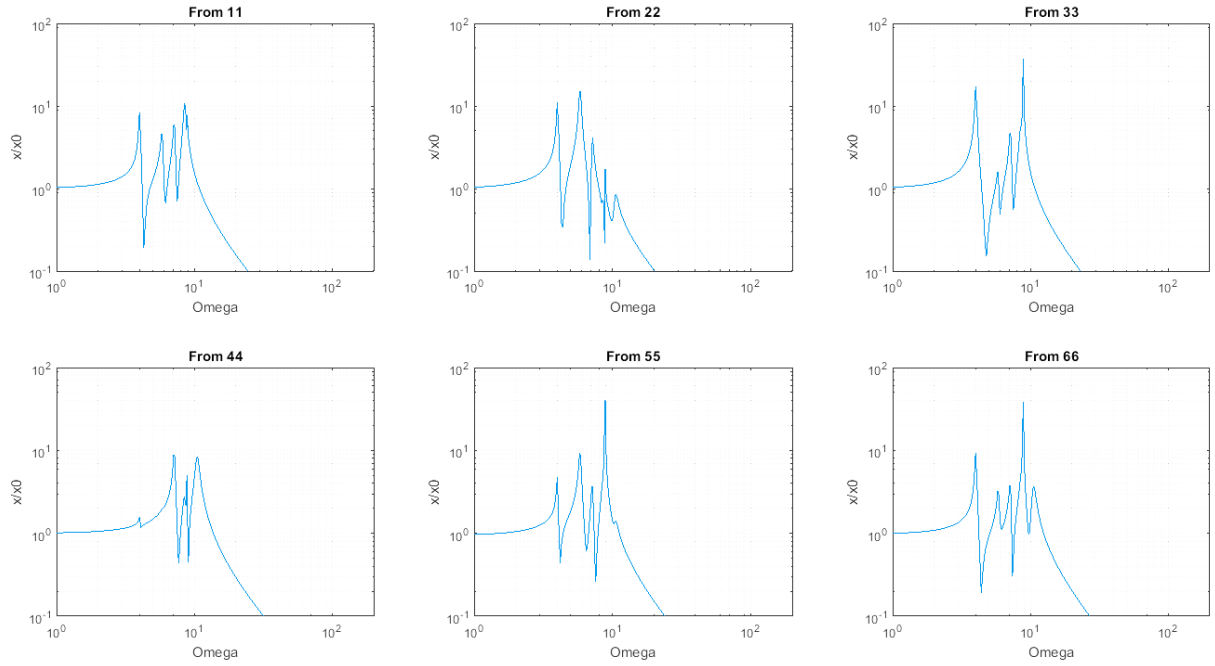

Figure 4-26, Enlarged transfer functions diagonal

In the transfer functions there are several peaks, these peaks are related to the eigenfrequencies of the system and can be made to be close to each other and close to the target isolation frequency. It shows that the vibration amplification zone will be larger than for a SDOF system and that therefore the target isolation frequencies have to be considered more precisely when designing 6DOF systems.

Table 6, Explanation of directions in figure

Number	Symbol	Direction
1	X	Surge
2	Y	Sway
3	Z	Heave
4	ψ	Yaw
5	ϕ	Pitch
6	θ	Roll

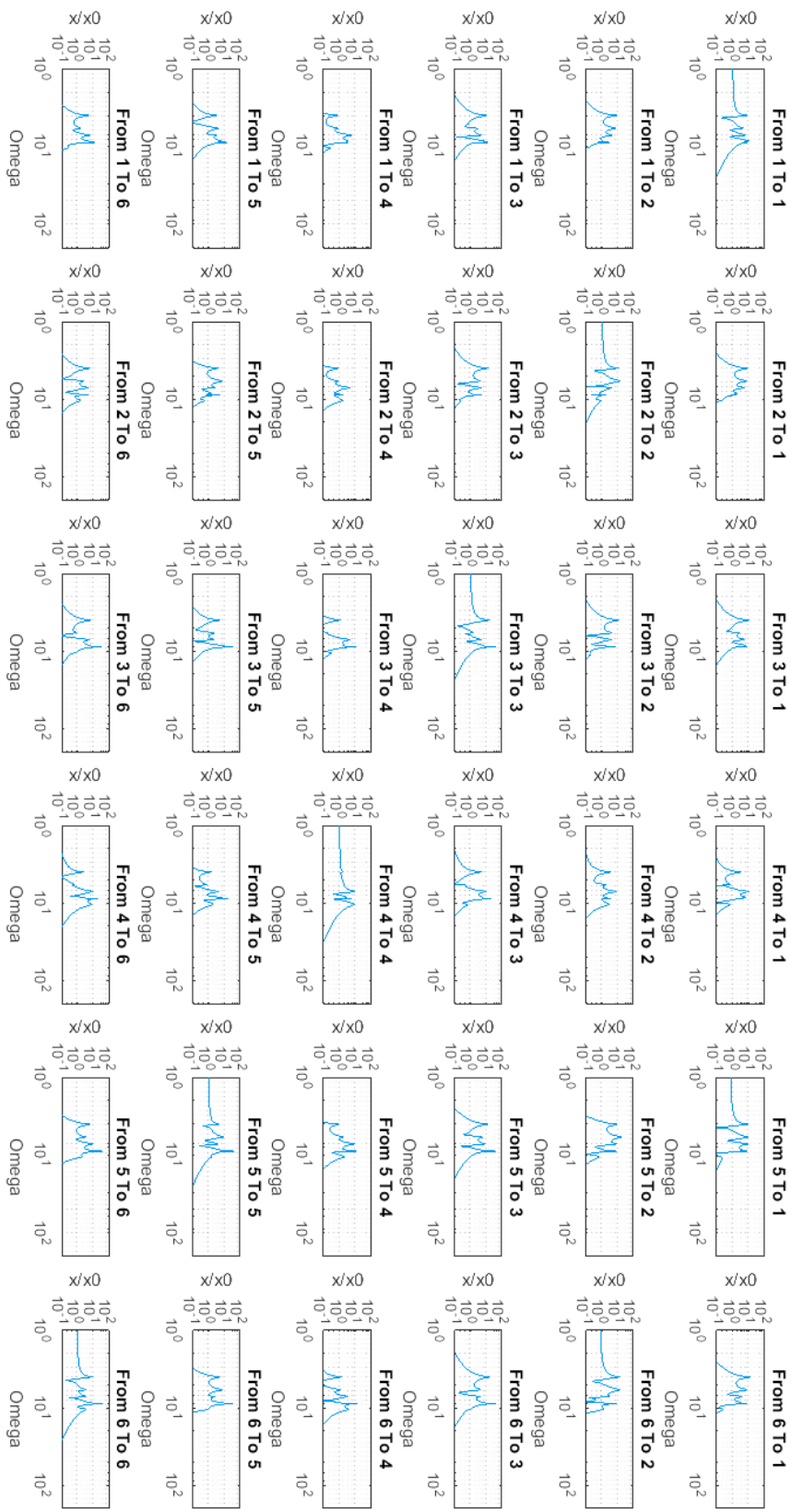

Figure 4-27, linearized transfer functions

4.3.3 Phase angles

The phase angles are the second half of the bode plot. In Figure 4-28 the diagonal s are displayed and in Figure 4-29 all phase angles are displayed. The diagonals are regarding the phase angle of a motion in direction of the base to the motion of the payload in that direction. For more information see section 4.3.2 and Table 6.

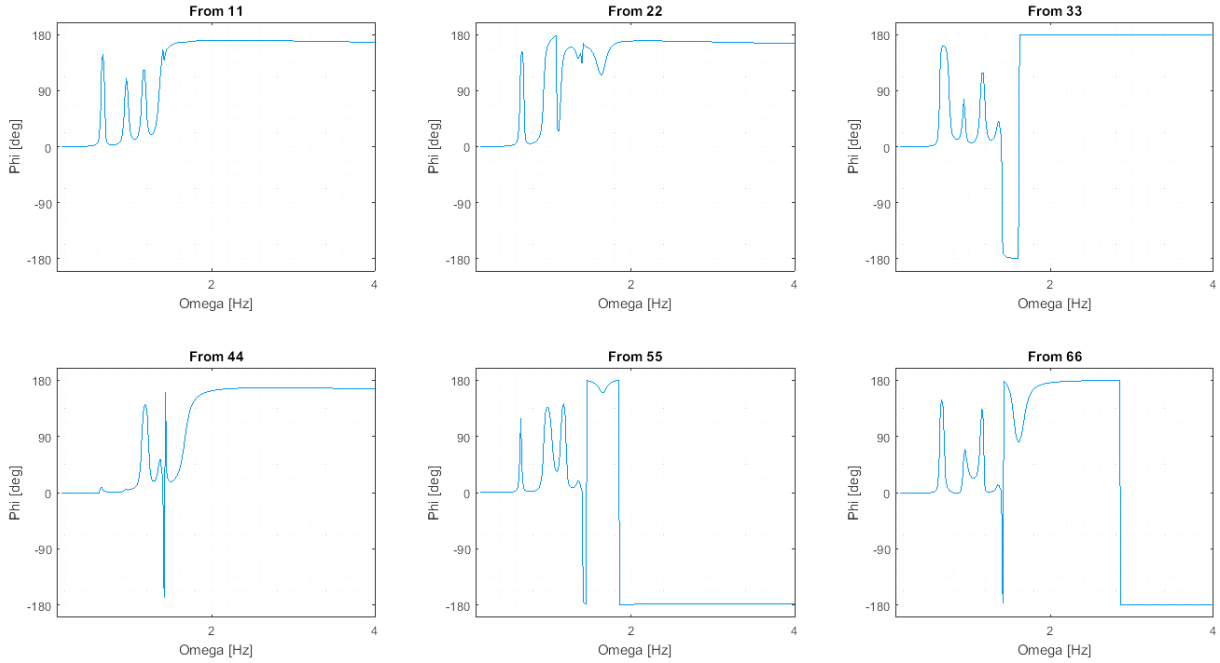

Figure 4-28, phase angles diagonal

In the figures it can clearly be seen that there are several peaks or jumps in the phase angles. These peaks and jumps coincide with the eigenfrequencies of the system. In these figures it is shown that the phase angle will vary greatly between the shift in frequencies, these phase shifts can be used to more easily determine what mode the system behaves in.

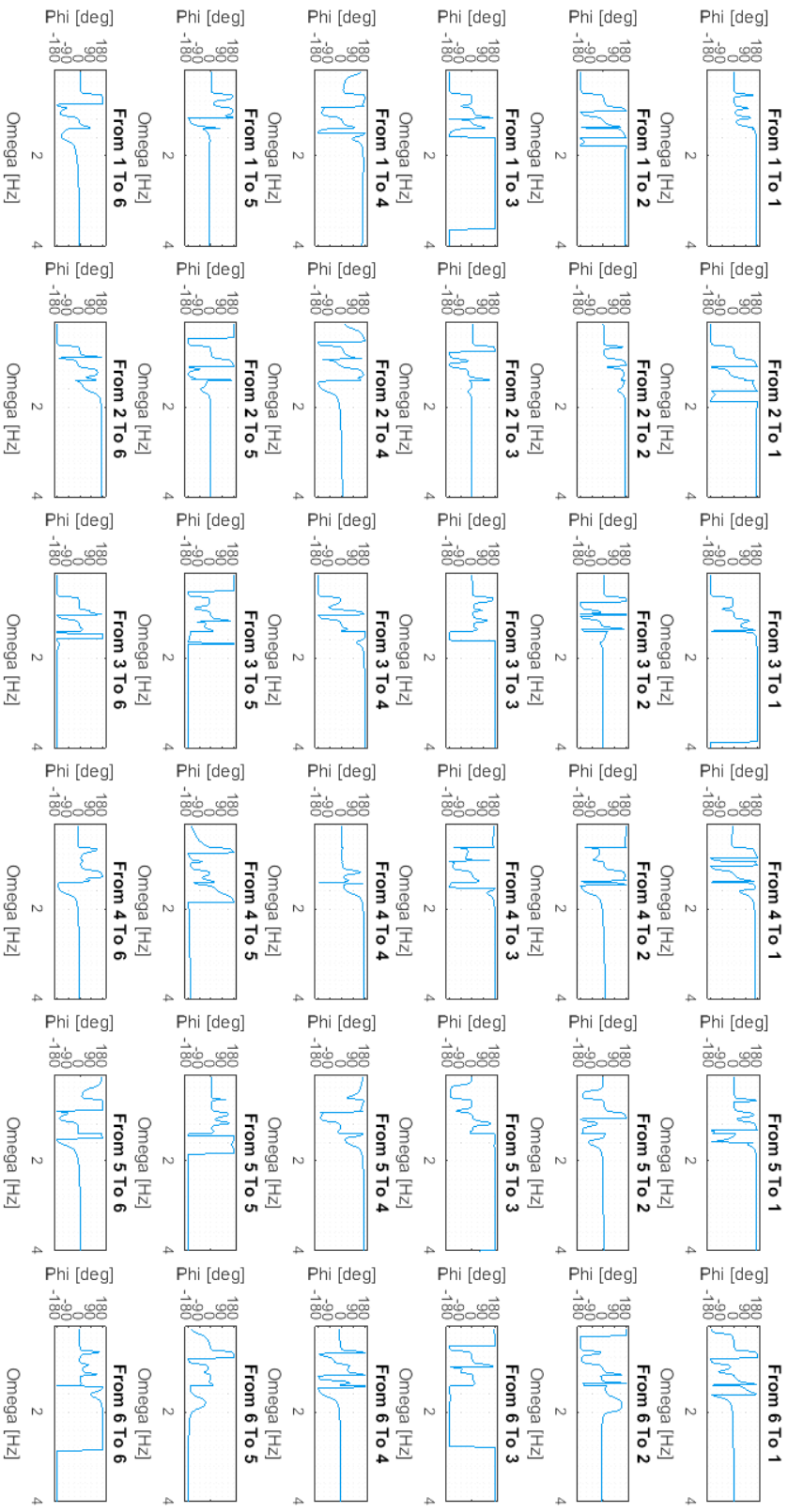

Figure 4-29, linearized phase angles

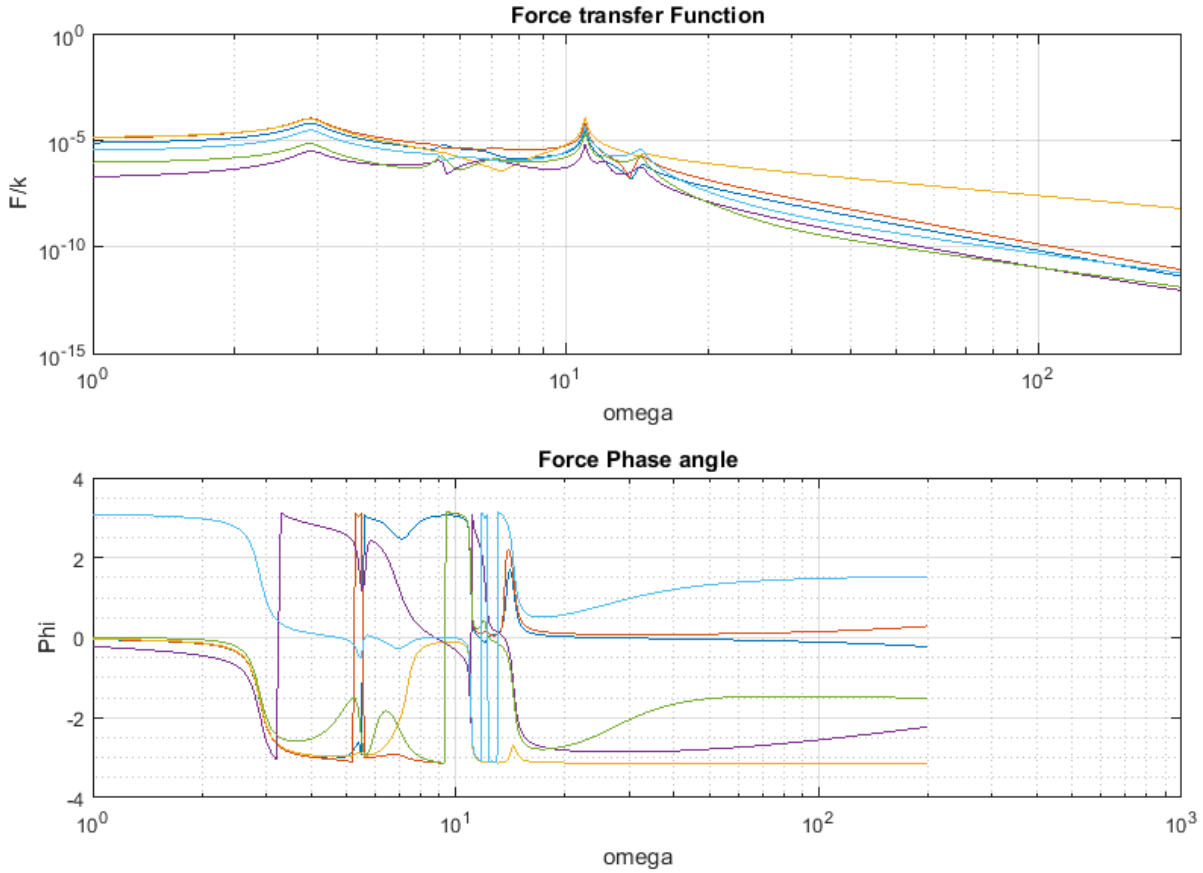

Figure 4-30, Direct loading bode plot

4.3.4 Time series

A number of time series simulations was run, these time simulations were done with a from which the transfer functions were determined. this was done in a similar manner to the simulations described in section 4.2.

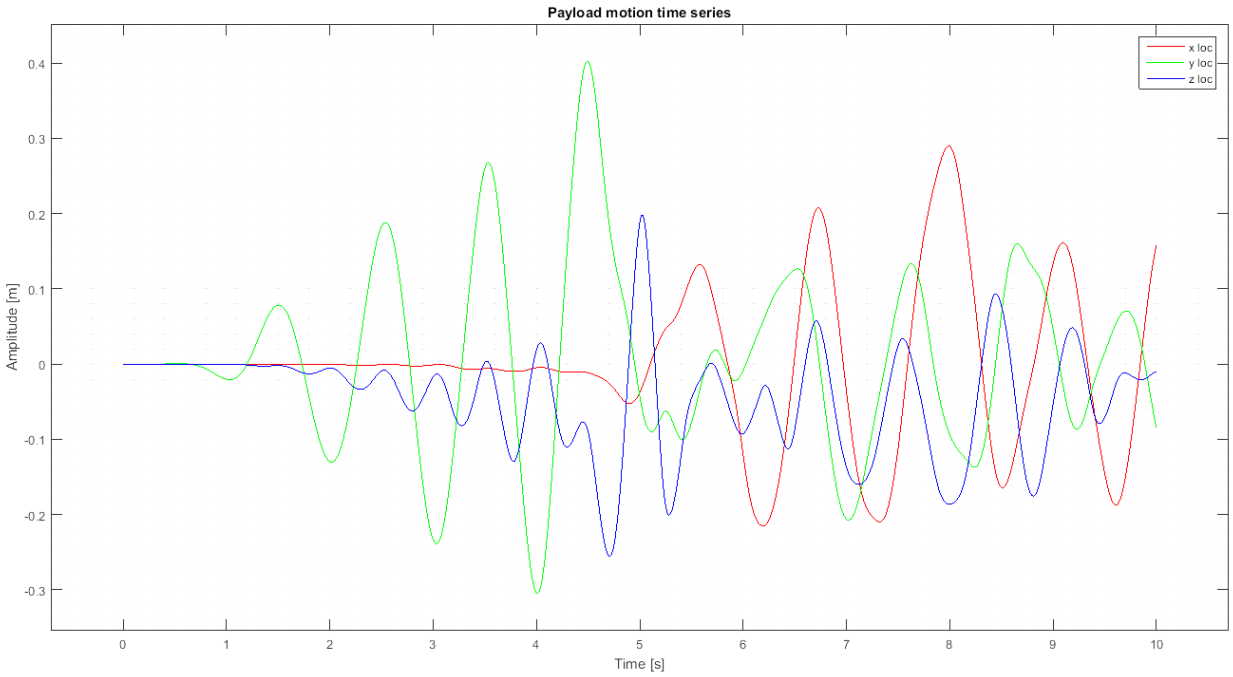

Figure 4-31, Example time series of the CoG translations

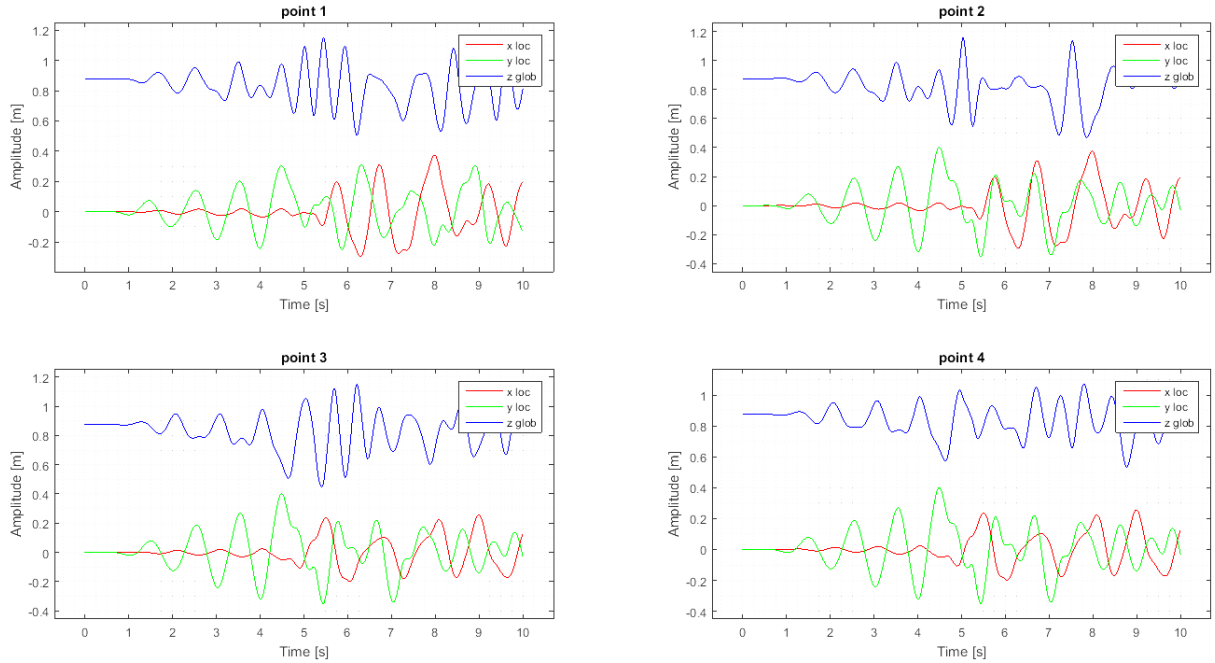

Figure 4-32, Four corners time series

In the case of a three dimensional payload the rotations affect the corners mostly as a translation. This translation is what affects the springs and NSM.

4.3.5 Non-linear transfer function

The transfer functions are obtained by applying a motion to the base of the structure in the Heave, Surge and Sway directions. Rotations in the base are disregarded due to the fact that the vessel will only have rotations due to very long waves and the frequency of these waves is of no interest to the vibration isolation question.

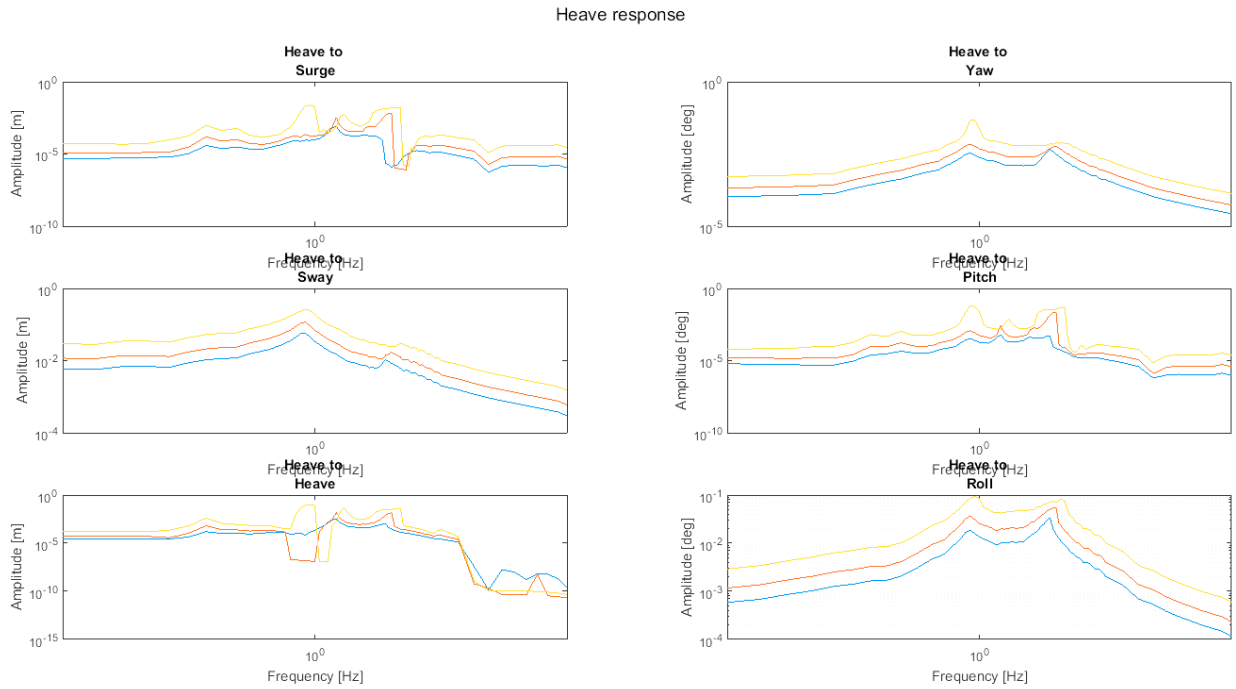

Figure 4-33, Transfer functions of the response to heave motions of the base

The responses are to a base excitation there are three base excitations, this is shown in the legend (Figure 4-34).

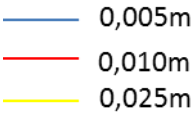

Figure 4-34, legend for Figure 4-33 to Figure 4-39

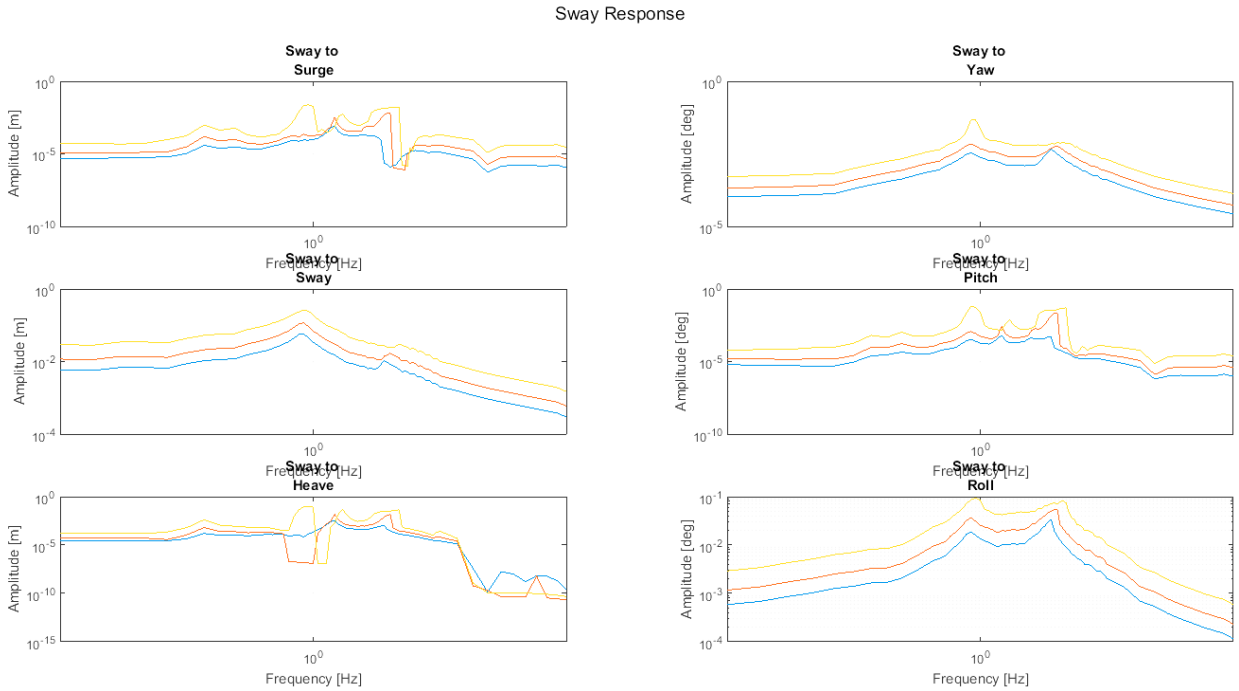

Figure 4-35, Transfer functions of the response to sway motions of the base

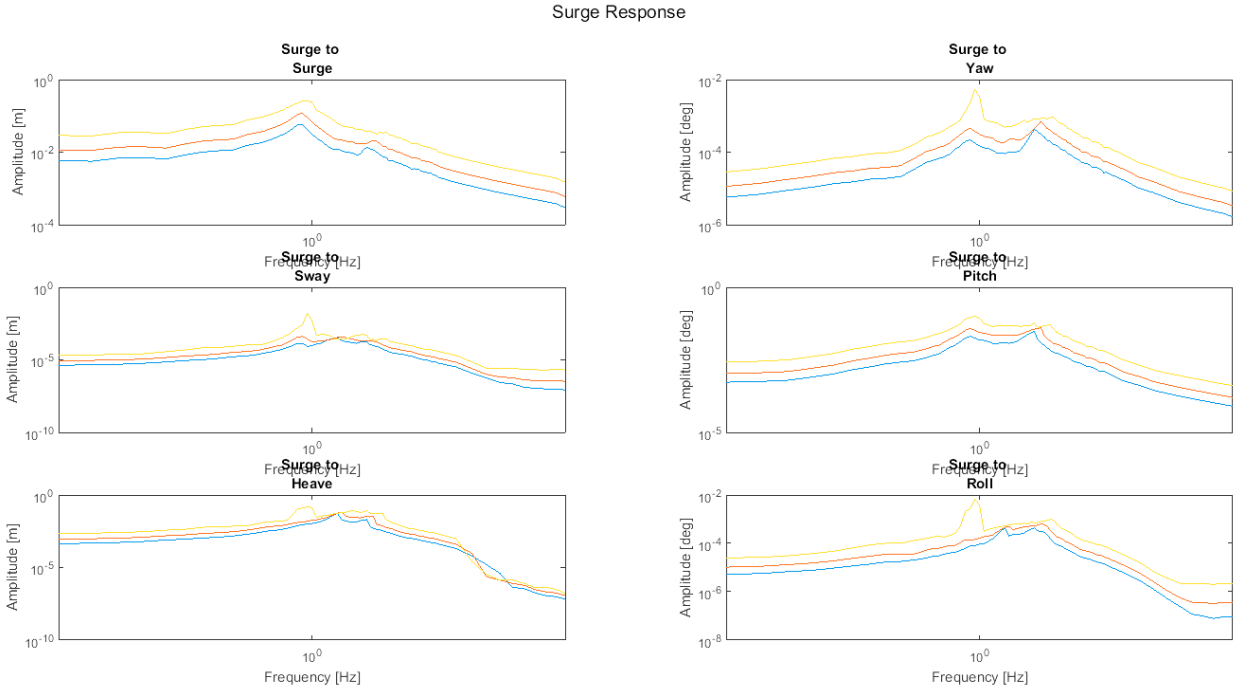

Figure 4-36, Transfer functions of the response to surge motions of the base

The normalised response is the response at a certain frequency divided by the input amplitude. The normalised response is given below. These figures are the proper transmissibility.

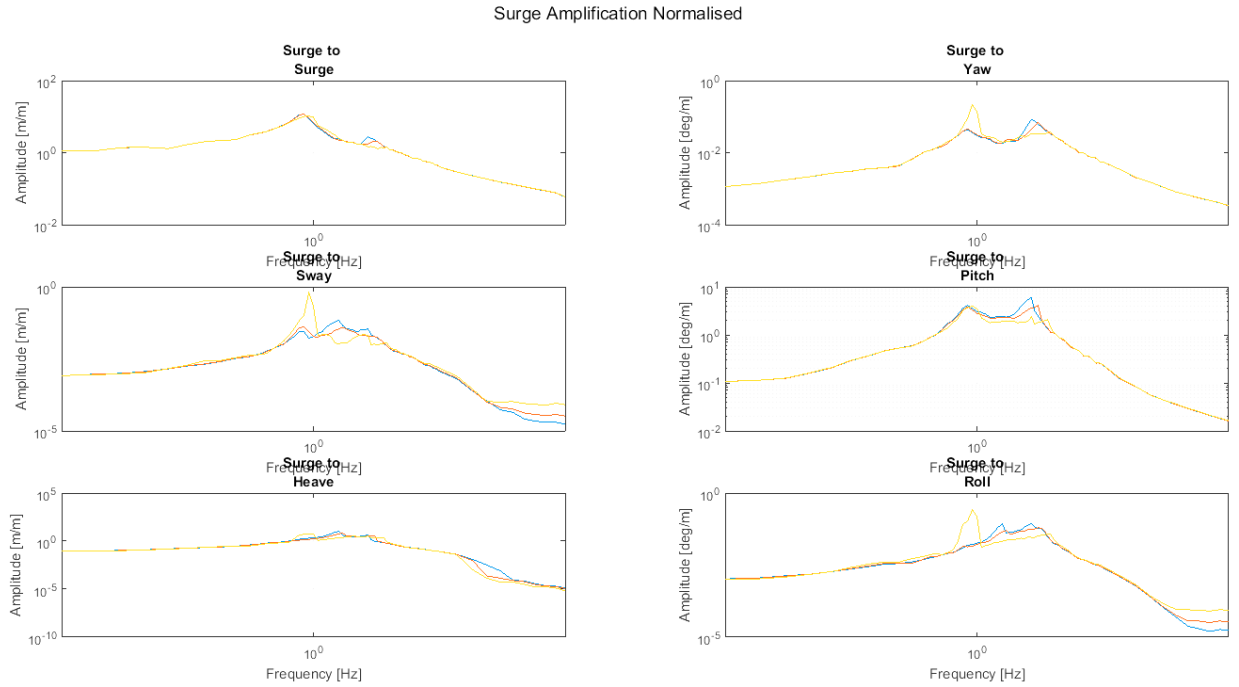

Figure 4-37, Transfer functions of the response to surge motions of the base - normalised

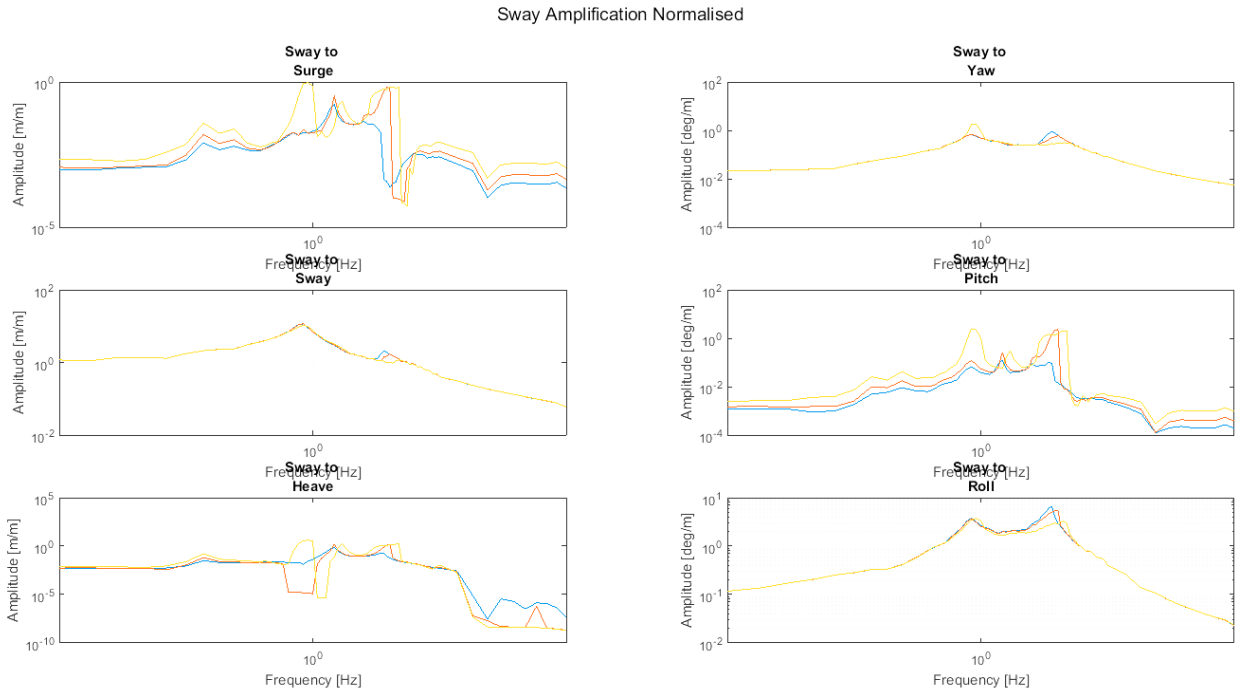

Figure 4-38, Transfer functions of the response to sway motions of the base - normalised

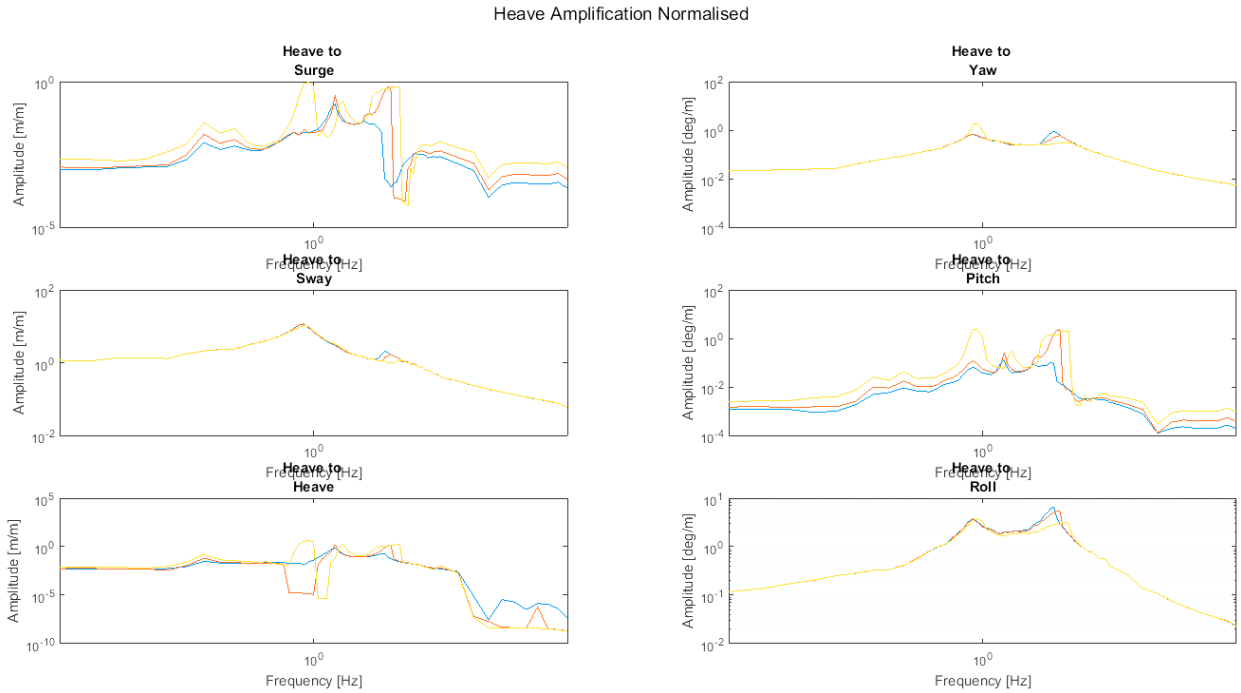

Figure 4-39,Transfer functions of the response to heave motions of the base – normalised

From the figures there can be seen that the transmissibility to and from most modes very low is. This results in a very nice vibration isolation behaviour in the considered system.

4.3.6 Conclusions

The six degrees of freedom system is more susceptible to the effects of the non-linearity due to the fact that there are already several peaks in the transfer function thus having an increased spread of the amplification zone. The increased spread of the amplification zone associated with the more severe non-linear behaviour as is shown in section 4.2 will limit the options for the bar length $[L]$. However, the results do show that the system can be used in practice; the higher frequencies are properly isolated, there are no signs of instability and the vibration amplification zone is within the target isolation zone.

5 Practical implementation

In this section the practical aspects of the NSM are discussed. The practical aspects centre around the creation of a prototype and the implementation on a dredge vessel. A prototype is required to validate the theories and assumptions regarding the creation of an NSM and the creation of the numerical model. The implementation is about the combination of more than one NSM and the low stiffness horizontal isolation.

5.1 Prototype

The theory developed in section 4.1 is valid for a system in which the hinges are frictionless and the damping is linear and proportional to the low eigenfrequency of the NSM. Another assumption is that there are no geometrical deviations. The damping $[\zeta]$ is set at 3% for an eigenfrequency of 1 Hz. The assumptions might not be valid and will be investigated using a prototype. The prototype can then be used to determine whether a different approach is necessary.

5.1.1 Design

Based on the theory of section 4.1 the design of a NSM was made. In Figure 5-1 a schematic design is shown for a mechanism which only has a single DoF. This is done by attaching the mass to a four bar mechanism with parallel horizontal arms. The four bar mechanism allows only vertical movement assumed that the displacement $[z]$ is not too large.

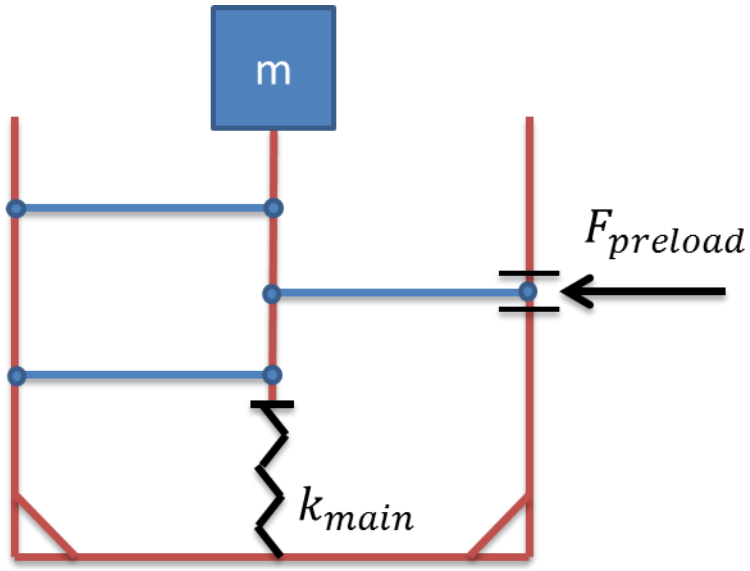

Figure 5-1, Schematical 1DoF test model

Application of the preload is done through a lever that transfers a vertical load through a hinged connection to the bars.

Figure 5-2, Parts for the NSM

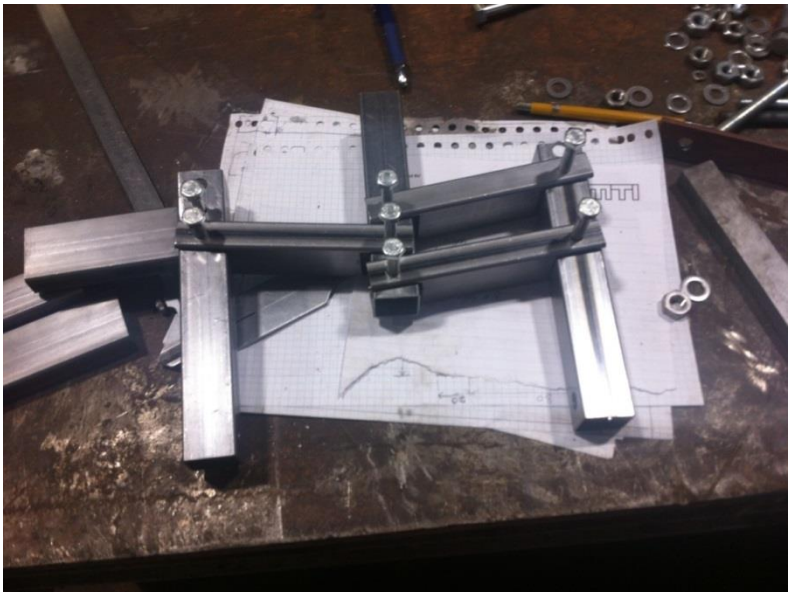

Figure 5-3, partly assembled NSM

Figure 5-4, Added top tension element

Figure 5-5, Loaded and levelled NSM

Figure 5-6, complete setup of NSM

5.1.2 Results

When the mechanism was finished it was tested with a mass of 5kg and a spring with a stiffness of approximately 450 N/m. The stiffness of the spring was measured by taking the initial length, applying a load of 5kg and measuring the deformed length. The initial length minus the deformed length is the deformation; ΔH which yields the following stiffness:

$$k = \frac{m \cdot g}{\Delta L} \tag{81}$$

The vibration was induced manually as a direct load. The eigenfrequency was estimated around 1.5Hz. this was confirmed by doing measurements over several oscillations. When there is no preload the oscillation is smooth and hardly requires any direct loading.

When a preload was applied the frequency could be reduced from 1.5Hz to approximately 1Hz. The preload and the direct load were applied by hand. In this case the mass would still oscillate however some significant direct load had to be applied to keep the oscillations perpetuating. The dissipation was investigated and the initial assumption of friction losses was confirmed. Next to the friction there were unexpected equilibrium points one at the zero point due to the fact that this is a four bar mechanism and the friction combined with a little skew of the bars was enough to create a stable point for the zero deflection point. When the mechanism is not properly aligned, a large preload (one that would not be sufficient to get overall negative stiffness of the system) will get the mechanism stuck in either the top or bottom equilibrium point. Additional attention will need to be paid to the fabrication tolerances and the reduction of friction in the system. The additional equilibrium point will not have a large impact in practice since this scenario can only occur when the system is adjusted and the preload is increased. When doing this a faulty setting resulting in the additional equilibria is easily noticed since the system is not in its usual centre point. The friction part of the NSM has been identified in literature before (Foss).

5.2 Implementation

The implementation of an NSM on a dredge vessel is difficult due to a number of factors namely the geometrical fit and the choices for distribution of the DoFs over the isolators.

5.2.1 Isolators and degrees of freedom

In theory it is possible to isolate the OC on a single system that takes care of all six DoFs in a single system. It is also possible to have a single degree of freedom to be isolated by a single system of a set of systems. One example of a 6DoF isolator is a large block of rubber underneath a mass.

An example of a system in which all DoFs are isolated by a single isolator is a mass on sliding springs with rotational springs attached for the rotations. In the case of the OC the choice is made to isolate the vertical directions separately because of the gravitational deflection (see section 2.1.3). In Figure 5-7 the choices regarding the positioning of the isolators are illustrated. Due to the size of the OC in relation to the displacement the rotations at the corners of the OC are disregarded. This means that the rotations of the OC are countered by a spring force in the direction of the spring and not a rotation of the head of the spring.

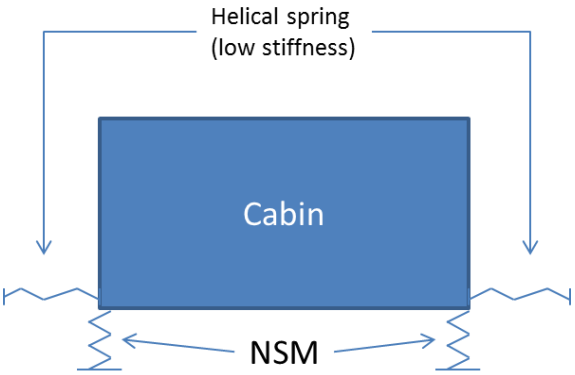

Figure 5-7, 2D illustration of isolation choices

5.2.2 Geometrical fit interior NSM

On paper the NSM looks quite slender and lean, however the forces passing through the bars and springs can become quite large and the connections to the hinges will become extremely crowded. Therefore the geometrical fit of the different parts of the NSM in relation to each other are important. The consequence of not doing this properly is that the designed mechanism cannot be utilised and is therefore worthless. In section 5.2.1 the degrees of freedom per isolator are determined therefore the manner in which the NSM has to be attached to the OC and the vessel are already limited.

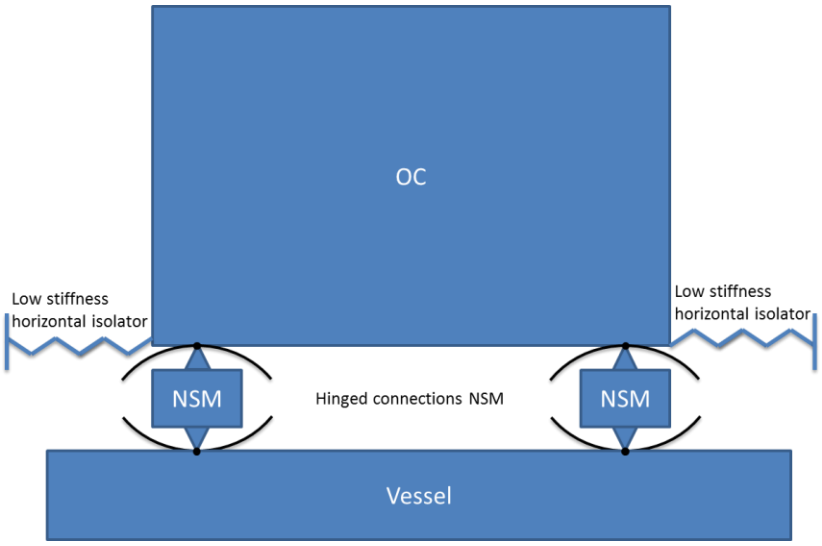

Figure 5-8, OC-vessel connection by NSM

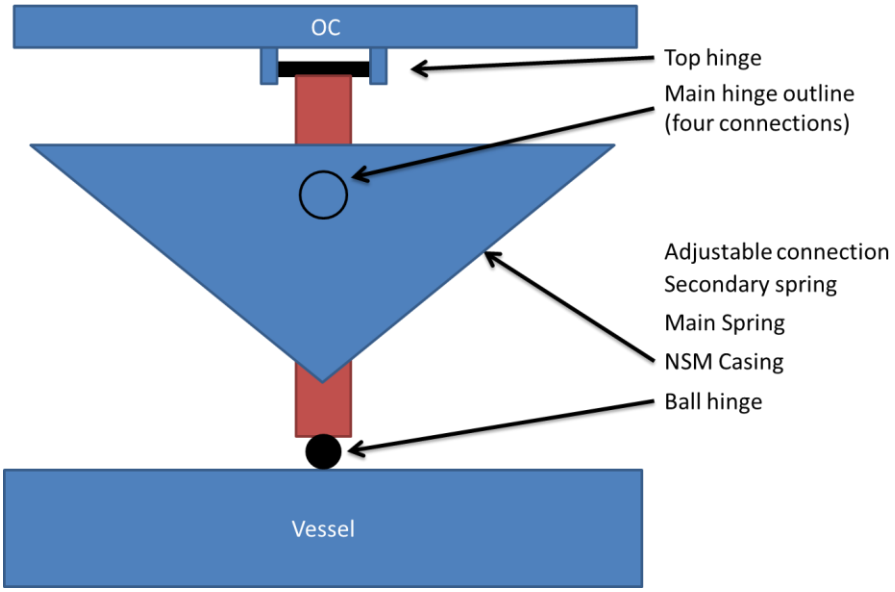

Figure 5-9, Schematic hinge locations of NSM

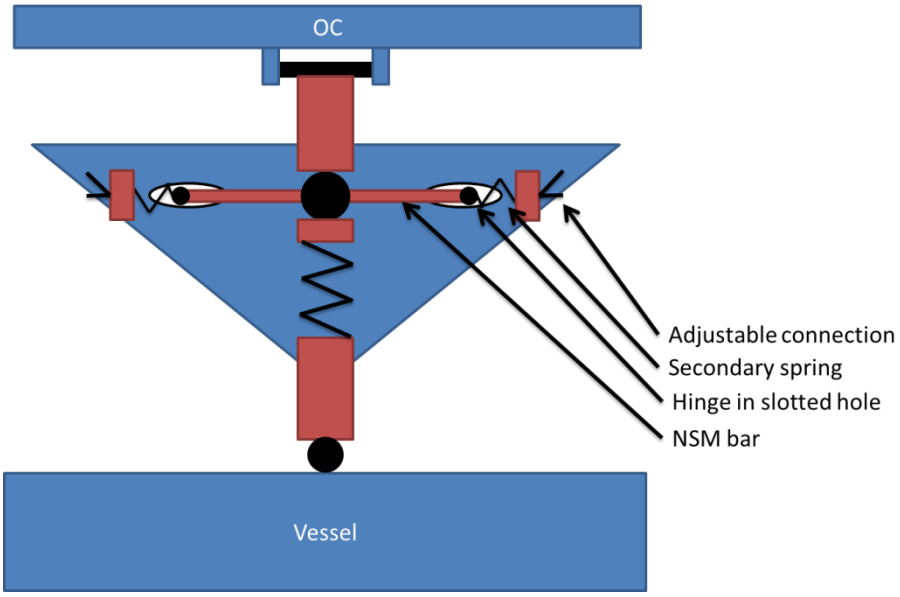

Figure 5-10, Inside NSM schematical

5.3 Conclusions

The original assumption of the low value of the damping is invalid for the prototype. When the design of a new prototype is done additional attention will need to be diverted to the identification and minimisation of the friction. The friction is dependent on the required preload. When designing the NSM it may be taken into account that for a smaller bar length, the required preload is also smaller. The use of friction as an additional energy dissipater is undesired due to the effect of friction on the vibration isolation behaviour, the isolation amplification zone will be larger and the reduction will be lower in the reduction zone.

The four bar mechanism that is used to design the prototype with one degree of freedom has a detrimental effect on the stability when the bars are not properly alligned. When the bars converge towards the central hinge, the preload is contributing to the stability thus requiring extra direct loading to perpetuate the oscillations. When the bars diverge an additional instability is added.

The optimal design has not yet been determined however several observations have been made regarding the parameters and dimensions. It is best to keep the bar length $[L]$ as low as possible while maintaining the clearance and limiting the non-linearity. The main spring stiffness $[k_1]$ is best to keep as low as possible while still maintaining load bearing capabilities, the preload $[P]$ is dependent on the stiffness and the bar length. The way the preload is setup allows for changes in the linearity of the system through the choices for the secondary stiffness $[k_2]$.

6 Conclusions

Cause of the current vibration issues is resonance. The resonance is caused by the overlap between the third natural frequency of the cutter and the operational frequency of the cutter. The isolation of vibrations at the source is impractical due to the fact that there are multiple sources at different locations. Application of isolation at the base of the cabin appears to be feasible. The other vibration sources are the engines and the waves. These two sources are also present in other vessels, for example, those used for shipping. Cutter vibrations require another type of isolation. This isolation can be designed to have an target isolation frequency in between the forcing frequency of the waves and the cutter. A Negative Stiffness Mechanism (NSM) was deemed the most promising and was investigated further in this thesis. Advantages of a NSM are: smooth out of range behaviour, low static deflection and components made of steel.

The NSM of the rigid bar type was chosen for further development. This mechanism can be designed to any specs that would be required. The parameters that can be used to design the mechanism are: bar length, mainspring stiffness, preload, secondary stiffness, preload length. One of the important dimensionless design parameters is the ratio between the deflection and the bar length. This parameter can be used to determine the non-linearity of a system. The effects of the non-linearity become more pronounced for the larger base excitation amplitudes. When this happens the amplification zone shifts into a higher frequency region. The model further indicates that the system can function properly outside the vibration isolation range relevant for the single degree of freedom system; the vibration reduction for a more linear system is significantly higher.

The optimal design has not yet been determined however several observations have been made regarding the parameters and dimensions. It is best to keep the bar length $[L]$ short while maintaining the clearance and limiting the non-linearity. The main spring stiffness $[k_1]$ is best to keep as low as possible while maintaining load bearing capabilities, the preload $[P]$ is dependent on the stiffness and the bar length. The way the preload is setup allows for changes in the linearity of the system through the choices for the secondary stiffness $[k_2]$.

There are less severe consequences of using the NSM. Some height will be added due to the current expected size of the NSM including hinges and movement space. The mounting platform on the vessels will have to be altered to accommodate the horizontal springs. The NSM can be disengaged by removing the preload which will increase the stiffness and thereby reduce the compliance.

7 Recommendations

In this section the recommendations for further research into negative stiffness mechanisms (NSM) will be presented. A number of assumptions was done to get an idea of the feasibility of using an NSM for vibration isolation of cutter dredgers. In case of future research these assumptions need to be revisited and checked. In this thesis the OC was considered to be a rigid mass which means that no deformation of the OC was occurring. The same was done for the deck of the CSD. Another assumption was that there was No OC- Vessel interaction due to disparity in weight, this assumption is likely not completely valid. The damping was assumed to be of low value and was taken into account as being linear is recommended that these assumptions are revisited.

A prototype with six degrees of freedom needs to be constructed. It is advised to make the NSM at true size due to the increasing importance of building tolerances when the size is reduced. The assumption done regarding the low value of the damping is not valid for the prototype. When the designing a new prototype; additional attention needs to be diverted to the identification an minimisation of the friction. It is recommended to find bearings with very low friction, high wear resistance and saltwater tolerance.

The detailed design for the NSM will need to consider proper material selection. For the material selection, it is recommended to use materials which have a high tolerance for saltwater and wear resistance, and to contact the production department about the manufacturing and costs. One of the obstacles for the detailed design are the hinge points, it is recommended to use one ball hinge and to split the other hinges into two separate bar hinges. This allows for more robust construction while maintaining the flexibility.

The uses of the NSM proposed in this thesis are limited to application in cutter suction dredgers. There are other applications available to increase the possible market. For marketing purposes it is advised to do some research into the safety aspects of an NSM compared to for example gas springs. If there is a safety advantage to the NSM the possibilities for mass use in the offshore market increase greatly.

8 Bibliography

Det Norske Veritas. (2004). part 6 chapter 15 Vibration class. In D. N. veritas, *rules and classification of ships.* Høvik: Det Norske veritas.

Det Norske Veritas. (2011). part 5 chapter 12 Comfort Class. In D. N. Veritas, *Rules for classification of ships.* Høvik: Det Norske Veritas AS.

Foss, G. C. (n.d.). A Low Stiffness Suspension System for Free-free modal testing. In G. C. Foss, *Boeing Defense & Space Group* (pp. 1402-1408). Kent, Washington, USA: Boeing Defense & Space Group.

Gopinah, K. (n.d.). Design of helical springs. In K. M. Gopinah, *Machine design II* (pp. 1-6). Madras: Indian Institute of Technology Madras.

International Standards Organisation. (2000). *ISO 6954:2000 Mechanical vibration — Guidelines for the measurement, reporting and evaluation of vibration with regard to habitability on passenger and merchant ships.* Geneva: ISO copyright office.

Lamancusa, J. S. (2002). Vibration isolation. In J. S. Lamancusa, *Noise Control* (pp. 12.1-12.14). Penn State.

Los, J. (2009). *Attenuating Vibrations with Negative Stiffness.* Delft: Delft university of technology.

Meijers, P. (1996). *Dynamica 3-A.* Delft: Delft University of technology.

Meriam, J. (1998). *Engineering Mechanics Dynamics.* Von Hoffmann Press Inc.

Platus, D. L. (1993, Februari 26). Smoothing out bad vibrations. *Machine Design vibration isolators*, pp. 123-130.

Royal IHC, MTI. (n.d.). *Internal Reporting.* Kinderdijk: Royal IHC.

Spijkers, J. (2005). *Structural Dynamics CT 4140 .* Delft: Delft University of Technology.

Stewart, R. H. (2006). Ocean Waves. In R. H. Stewart, *Introduction to physical oceanography.* College Station: Department of Oceanography, Texas A&M University .

Zahrai, S. M. (2009). Effect of impact damper on SDOF system vibrations under harmonic and impulsive excitations. *Journal of Physics*.